Atherosclerosis Treatment with Stimuli-Responsive Nanoagents: Recent Advances and Future Perspectives

Ali Maruf [a,†], Yi Wang [a,†], Tieyin Yin [a], Junli Huang [a], Nan Wang [b], Colm Durkan [b], Youhua Tan [c], Wei Wu [a,*], Gui-Xue Wang [a,*]

[a] Key Laboratory for Biorheological Science and Technology of Ministry of Education, State and Local Joint Engineering Laboratory for Vascular Implants, Bioengineering College of Chongqing University, Chongqing, 400030, China
[b] The Nanoscience Centre, University of Cambridge, Cambridge, CB3 0FF, UK
[c] Department of Biomedical Engineering, The Hong Kong Polytechnic University, Hong Kong SAR, China

[†] These authors contributed equally to this work.
* Corresponding authors:
E-mail addresses: wanggx@cqu.edu.cn (Gui-Xue Wang); david2015@cqu.edu.cn (Wei Wu)

Abstract

Atherosclerosis is the root of approximately one third of global mortalities. Nanotechnology exhibits splendid prospects to combat atherosclerosis at the molecular level by engineering smart nanoagents with versatile functionalizations. Significant advances in nanoengineering enable nanoagents to autonomously navigate in the bloodstream, escape from biological barriers, and assemble with their nano-cohort at the targeted lesion. The assembly of nanoagents with endogenous and exogenous stimuli breaks down their shells, facilitates intracellular delivery, releases their cargo to kill the corrupt cells, and gives imaging reports. All these improvements pave the way towards personalized medicine for atherosclerosis. This review systematically summarizes the recent advances in stimuli-responsive nanoagents for atherosclerosis management and its progress in clinical trials.

Graphical Abstract

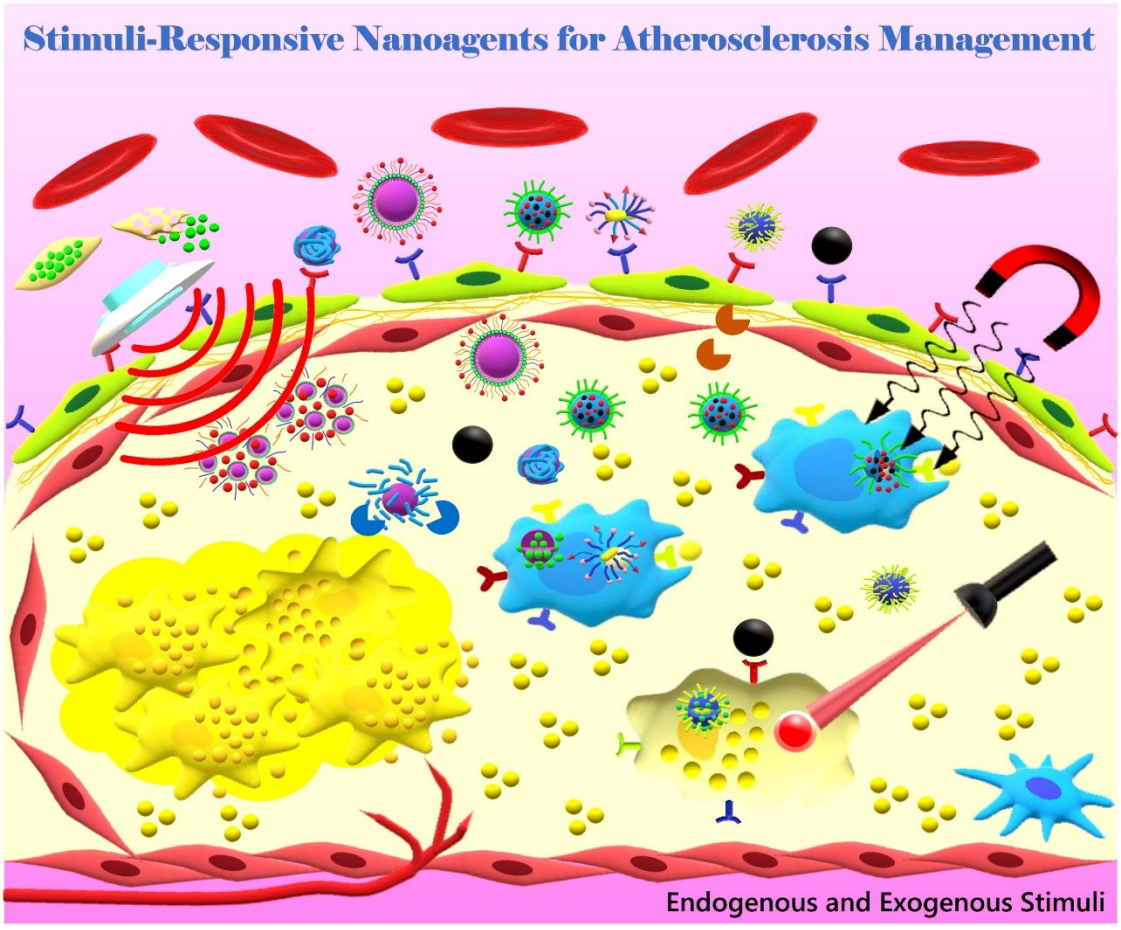

Author Biography

Ali Maruf finished his undergraduate from Gadjah Mada University, Indonesia (2012). He has a professional working experience in micro- and nano-encapsulation for three years with a number of outstanding awards. Currently, he is pursuing a graduate degree in Bioengineering College, Chongqing University, China supervised by Prof. Gui-Xue Wang and Assoc. Prof. Wei Wu. His current research focalizes on theranostic stimuli-responsive nanoagents, mechanosensitive nanovalves, and rubber-like microagents to treat vascular diseases and tumor.

Assoc. Prof. Wei Wu received his Ph.D. in biomedical engineering at Sichuan University, China (2015). He is currently an associate professor at Chongqing University. He has broad experience in the fields of the stimuli-responsive polymeric nanocarriers for antitumor therapy, the biomembrane coating nanomedicine, and the cardiovascular bioresorbable scaffold.

Prof. Gui-Xue Wang, Dean of the Bioengineering College of Chongqing University. His areas of research interests include cardio-cerebrovascular biomechanics and mechnobiology, hemodynamics and atherosclerosis, biomedical materials, nanomedicine, vascular implants. Other job titles include: Director of Key Laboratory of Biorheological Science and Technology, Ministry of Education, China; Director of State and Local Joint Engineering Laboratory in Vascular Implants, China; Executive Member of the Council, China Branch of International Society of Atherosclerosis; Associate Director, Branch of Atherosclerosis under Chinese Society of Pathophysiology.

1. Introduction

Atherosclerotic vascular diseases account for one third of global mortalities.[1] Atherosclerosis, known as a "silent killer", is the most common cause of cardiovascular diseases (CVDs), such as stroke and coronary artery disease. CVDs lead to nearly 18 million human deaths in 2016, 80% of which are due to myocardial infarction (heart attack) and stroke. More than 75% of CVD-induced deaths occur in low- and middle-income countries.[2] As a chronic disease, atherosclerosis is resulted from lipid-deposition-mediated hardening and narrowing of arteries that can reduce and gradually block blood flow.[3] An atherosclerotic plaque can develop and cover up to 90% of the lumen.[4] This narrowed vessel leads to changes in the blood flow pattern. The average shear stress is 15 dyn cm^{-2} in a healthy coronary artery, which can be elevated to 70-100 dyn cm^{-2} or even higher by such blockages at the site of advanced lesions.[5] In addition, atherosclerosis preferentially develops within the branching and curved sites of the artery and is influenced by low and oscillatory shear stress (OSS) that mediates low-density lipoprotein (LDL) uptake in endothelial cells. This indicates that hemodynamics plays an important role in the establishment of atherosclerosis.[6] Atherosclerosis starts to develop in the early teenage stage and evolves thereafter. Regardless of the similar progression of atherosclerosis in different races, genders, and geographic locations, the rate of progression in atherosclerosis is faster in patients with risk factors such as hypertension, tobacco smoking, diabetes mellitus, obesity, and genetic inclination.[7]

At the cellular level, the endothelium plays key roles in protecting blood vessel walls, participating in inflammatory reactions, secreting proteins on its surface to prevent blood clotting, and developing new blood vessels (angiogenesis).[8,9] Atherosclerosis can be triggered when the endothelium is damaged by high blood pressure (hypertension)[10] and toxins (e.g. smoking[11] and high glucose levels or hyperglycemia).[12] The process is accelerated if there is insufficient high-density lipoprotein (HDL) to remove cholesterol from tissues and carry it back to the liver, known as reverse cholesterol transport (RCT).[13] High ratio of LDL and HDL (more than 3:1) induces high levels of cholesterol in the blood or hypercholesterolemia, which may trigger endothelial dysfunction and promote the accumulation of LDL in the sub-endothelial space.[14-16] The injured or dysfunctional endothelium

expresses various adhesion molecules, including endothelial selectin (E-selectin), intercellular adhesion molecule-1 (ICAM-1), and vascular cell adhesion molecule-1 (VCAM-1), which can capture monocytes and allow them to extravasate into the tunica intima (sub-endothelial space).[17,18] Free radicals, especially superoxide anions, are released from the damaged endothelium and macrophages in response to LDL accumulation.[19,20] The excessive generation of reactive oxygen species (ROS) promotes oxidative stress[21] and the formation of oxidized LDL (Ox-LDL).[22] The dysfunctional endothelium releases macrophage colony stimulating factor (M-CSF)/colony stimulating factor-1 (CSF-1) that can differentiate monocytes into macrophages.[23,24] These macrophages then engulf Ox-LDL via scavenger receptors (scavenger receptor type A (SR-A), CD36, and lectin-like oxidized low-density lipoprotein receptor-1 (LOX-1))[25] and become foam cells due to the excessive intracellular accumulation of cholesterol.[26] Macrophages are also involved in the activation of T-lymphocytes[27] by recruiting them into the tunica intima and releasing TNF-α and INF-γ that amplify the inflammatory response.[28] The initial accumulation of macrophage-derived foam cells forms a lesion called fatty streak.[29]

The dysfunctional endothelium and macrophage-derived foam cells secrete fibroblast growth factor (FGF) and platelet-derived growth factor (PDGF) that attract vascular smooth muscle cells (VSMCs) from the tunica media to migrate to the tunica intima and stimulate their proliferation together with the cytokines secreted by macrophages.[29,30] VSMCs then synthesize collagen, proteoglycans, and elastin leading to the formation of a fibrous cap to prevent blood clotting[31,32] and become vascular smooth muscle-derived foam cells by accumulating Ox-LDL.[33,34] In response to the excessive accumulation of lipids, dying macrophages release free cholesterol and cellular components in the tunica intima.[35] Lipid-laden macrophages and VSMCs then create a lipid core, which has a soft and rupture-prone property due to the accumulation of free cholesterol from the necrotic-foam cells.[36] The vascular smooth muscle-derived foam cells also deposit calcium and eventually lead to the creation of calcium crystals in the tunica intima, which makes the plaque rough and hard (intimal calcification process).[37] Taken together, the developments of fibrous cap, lipid

core formation, and calcification generate a stable atherosclerotic plaque. At this stage, small feeding blood vessels grow into the plaque (neovascularization) due to the hypoxic condition.[38] These microvessels also play an important role in intraplaque hemorrhage and lipid core progression.[39] At the advanced stage of plaque development, the fibrous cap erodes considerably due to the increased activities of matrix metalloproteinases (MMPs), especially MMP-2 and MMP-9, that can degrade extracellular matrices (ECM).[40] Finally, high shear stress and ECM degradation in fibrous caps induce the formation of a vulnerable plaque that is prone to rupture and can cause atherothrombosis.[41-44]

Traditionally, angioplasty and stenting have been implemented for advanced atherosclerotic patients for a number of years, especially when medical therapy fails. However, there are two major risks of placing a bare metal stent in atherosclerosis treatment, namely in-stent restenosis (ISR) and stent thrombosis (ST). Therefore, a number of techniques have been developed to overcome these limitations, such as high nitrogen nickel-free austenitic stainless steel for coronary stents[45] and stent coatings with mesenchymal stem cells, SiCOH plasma, and CD133 antibody to improve re-endothelialization and anticoagulation properties and reduce ISR.[46-48] To further suppress ISR, drug-eluting stents (DESs) have attracted much attention nowadays. However, the delayed re-endothelialization, inflammation, and hypersensitivity of DESs can induce late ST, thereby raising the long-term safety concern.[49-50] To tackle this problem, elemene, arsenic trioxide, docetaxel, and rapamycin (RAP) have been utilized as drug candidates in DESs; multiple layer coatings using platelet glycoprotein IIb/IIIa receptor antibody SZ-21 and poly-L-lactic acid (PLLA) can suppress ISR, promote rapid re-endothelialization, and inhibit VSMC proliferation.[51-54] In addition, biodegradable polymers are now being tested as the stent material.[55] Nevertheless, ISR still occurs in about 10% of angioplasty patients after the treatment with the second-generation DESs with 0.8% to 2.9% ST rate.[56]

To overcome these problems, the development of more effective and promising treatments is necessary and can be achieved through nanomedicine. This burgeoning field applies

nanotechnologies to healthcare and medicine,[57] and employs nanoagents to enhance the effectiveness of drugs and/or imaging molecules with diminished side effects to non-targeted cells, tissues, and organs. Due to the rapid development in multifunctional nanomedicine, nanoagents can be exploited to meet the demands of simultaneous imaging and therapeutic functions, known as theranostic nanomedicine,[58] which has shown the promising prospect for atherosclerosis management over the last decade. Recently, nanoagents with small sizes (around 50-100 nm) have become a research hotspot in atherosclerosis management, as they persist in blood circulation longer than larger-size nanoagents leading to better drug delivery and molecular imaging outputs.[59] However, to further improve the delivery efficiency and safety of nanoagents, nanoagents and drugs need to be integrated into diverse stimuli-responsive systems that can fine-tune the nanoagents and release the drugs to the specific targeted sites for the treatment of corrupt cells.[60]

A number of organic and inorganic materials have been designed to meet the demands of stimuli-responsive systems. Star polymers, for instance, which have unique topological structures and attractive physical/chemical properties, can be devised to be pH-, enzyme-, redox-, light-, and temperature-responsive for targeted drug and gene delivery.[61] Moreover, a hybrid system promises multifarious properties in nanomedicine due to the combination of organic and inorganic materials. One widely-used inorganic nanoparticle is mesoporous silica nanoparticles (MSNPs) due to high drug loading capacity, superior stability, excellent biocompatibility, low tangible cytotoxicity, high surface area, uniform dimensions, and facile surface modification.[62] Decoration with other materials, such as poly(ethylene glycol) (PEG) as a dispersity-enhancer and poly(2-(pentamethyleneimino)ethyl methacrylate) (PPEMA) as an ultra-pH-sensitive gatekeeper, can remotely open and close their nanometer-size pores and thus build an intelligent stimuli-responsive nanosystem for controlled drug release.[63]

To date, much attention has been focused on stimuli-responsive nanoagents (SRNAGs) to improve the diagnosis and therapy of atherosclerosis. To the best of our knowledge, most of the existing reviews summarize the applications of SRNAGs mainly for general cardiovascular diseases and

cancer therapy, while only a very limited number of them focus on atherosclerosis management. Therefore, this review highlighted the recent advances in SRNAGs that are responsive to endogenous (ROS, enzymes, pH, and shear stress) and exogenous stimuli (light, ultrasound, and magnetic field) for effective atherosclerosis treatment and further summarized the progression of SRNAGs in clinical trials.

2. Nanoparticle Design Aims

Both organic and inorganic nanoparticles have attracted tremendous attention in biomedical fields as they can be modified in such a way as to escape biological barriers and target specific tissues for drug delivery. Organic nanoparticles are represented by polymeric nanoparticles, micelles, liposomes, nanogels, and dendrimers; whereas inorganic nanoparticles consist of MSNPs, magnetic nanoparticles (MNPs), gold nanoparticles (AuNPs), quantum dots (QDs), and carbon nanotubes (CNTs).[64-67] To synergistically combine their advantages, organic and inorganic nanoparticles can be incorporated in nanoassemblies, referred to as hybrid nanoparticles.[68] Various methods, such as polycarbonate membrane extrusion, sonication, dialysis, microemulsion, self-assembly, and sol-gel techniques, can be used to synthesize nanoparticles.[69-71] The ultimate aims of nanoparticle design are for (i) targeting, (ii) controlled drug release, (iii) enhanced imaging, and (iv) theranostics.

To improve the delivery efficiency, it is important to design a nanoparticle that can essentially function like a robot and deliver drugs to the targeted sites. In general, there are two main methods to navigate nanoagents to diseased sites, namely passive- and active-targeting.[72] Passive targeting is mediated by the enhanced permeability and retention (EPR) effect,[73] while active targeting employs ligands such as antibodies, sugars, or peptides, which bind to the specific receptors overexpressed at the targeted lesions.[74] Recent findings show that only 0.7% of administered nanoparticles can be delivered to the targeted diseased tissues,[75] suggesting the necessity in refining the nanoparticle design to enhance the delivery efficiency.

The drugs should be released by the nanocarriers in a controllable manner as the drug concentration should be maintained between the minimum effective concentration (MEC) and the minimum toxic concentration (MTC).[76,77] It is thus paramount to equip nanocarriers with the "on-demand" cargo-releasing properties to achieve spatial-, time-, and dosage-controlled drug release profiles via diffusion-, solvent-, degradation-, or stimuli-controlled manner.[78-80] For instance, pH-responsive micelles based on amphiphilic diblock copolymer poly(2-diisopropylaminoethyl methacrylate)-*b*-poly(2-aminoethyl methacrylate hydrochloride) (PDPA-*b*-PAMA) could release drugs swiftly after a contact with the intracellular acidity of endo-/lysosome (pH values of 5.5-6.0 and 4.5-5.0, respectively).[81-84]

The potential of nanoparticles as agents for molecular imaging is continuously growing, alongside the need to develop better imaging techniques, improve imaging quality, and facilitate multimodal imaging for precise diagnosis.[85] Instead of Positron Emission Tomography (PET) that uses radionuclides, such as ^{18}F, ^{11}C, ^{13}N, and ^{15}O and Single Photon Emission Computed Tomography (SPECT) that uses radioisotopes, such as ^{99m}Tc, ^{123}I, and ^{131}I, recent developments of contrast agents allow Magnetic Resonance Imaging (MRI),[86] Contrast-Enhanced Ultrasound (CEUS) Imaging,[87] Near-Infrared Fluorescence (NIRF) Imaging,[88] and Photoacoustic Imaging (PAI)[89] as molecular imaging modalities, which can be combined to achieve multimodal imaging.[90]

Importantly, the development of theranostic nanomedicine allows us to assess the drug delivery efficiency by imaging modalities and their therapeutic effects. Some nanoagents, such as AuNPs,[91] iron oxide nanoparticles (IONs),[92] and copper sulfide nanoparticles,[93] possess a theranostic profile in a single particle and thus hold the potential for low-cost and effective nanomedicine. In addition, the superior properties of theranostic nanoagents can help clinicians to identify patients with a unique molecular phenotype and positive indications upon treatment, supporting the applications of nanoagents in personalized medicine.

3. Applications

In atherosclerosis, the acidic microenvironment, elevated shear stress, extracellular enzymes, and increased ROS production can be used as endogenous stimuli to fine-tune the SRNAGs for cargo release or inhibition of pro-atherosclerotic enzymes. Furthermore, exogenous stimuli such as light, magnetic field, and ultrasound can be utilized to activate SRNAGs for cargo delivery, treatment (such as photodynamic/thermal therapy), and imaging. Moreover, SRNAGs can be subtly designed to be responsive to more than one stimulus, which will enhance the potential of SRNAGs to target specific cells, such as endothelial cells, monocytes/macrophages, VSMCs, and foam cells in atherosclerotic lesions (**Figure 1**). Recent advances in theranostic SRNAGs were summarized in **Table 1**. In addition, some SRNAGs have entered phase 1 and 2 clinical trials. These stimuli-responsive systems will help to improve targeted drug delivery and safety profiles for precise diagnosis and therapy, which show great potential to support the applications of personalized medicine for atherosclerosis in the near future.

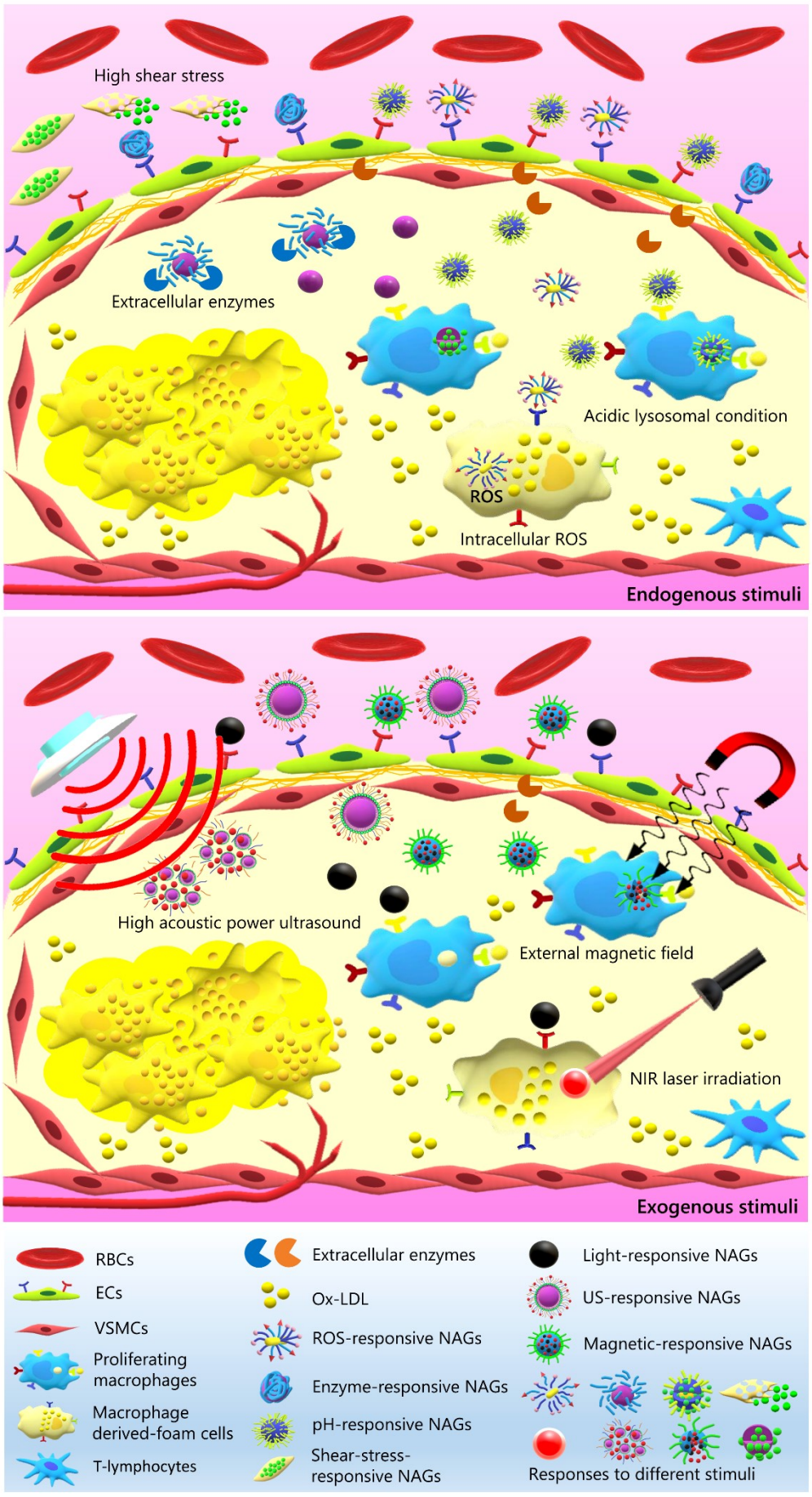

Figure 1. Schematic diagram of stimuli-responsive nanoagents (SRNAGs) for atherosclerosis management. RBCs: red blood cells; ECs: endothelial cells; VSMCs: vascular smooth muscle cells; Ox-LDL: oxidized low-density lipoprotein; ROS: reactive oxygen species; NAGs: nanoagents; US: ultrasound.

3.1. Endogenous Stimuli-Responsive Nanoagents

3.1.1. ROS Responsive

Reactive oxygen species (ROS) are a group of small and reactive molecules that modulate versatile cellular functions. ROS are pivotal for vascular homeostasis, but overproduction of ROS entails vascular damage.[21] The predominant ROS consist of free radicals such as superoxide ($O_2^{\cdot-}$) and hydroxyl ($HO^{\cdot}$) radicals and nonradical molecules such as hydrogen peroxide (H_2O_2), peroxynitrite ($ONOO^-$), and hypochlorous acid (HOCl).[94-96] Excessive levels of ROS promote oxidative alteration of lipoproteins (Ox-LDL), endothelial dysfunction, DNA damage, leukocyte migration and differentiation, VSMC proliferation, and collagen degradation by MMPs,[21] thus evidencing that excessive ROS generation can enhance the possibility of atherogenesis.

In fact, there are native ROS producing systems in atherosclerosis such as mitochondria enzymes,[96] uncoupled nitric oxide synthases,[97] lipoxygenases,[98] myeloperoxidases,[99] xanthine oxidases,[100] and NAD(P)H oxidases.[101] In response to high intra- and extracellular concentration of deleterious ROS, the cellular redox status is equilibrated by native antioxidants (reduced glutathione, ascorbic acid, α-tocopherol, and ubiquinol-10) and antioxidant enzymes.[95] These antioxidant enzymes include superoxide dismutases (SODs) that convert superoxide to hydrogen peroxide, catalases that alter hydrogen peroxide to water and oxygen, thioredoxins that reduce hydrogen peroxides and other target proteins, glutathione peroxidases, paraoxonases, and nitric oxide synthases.[102-105] The equilibrium between ROS generation and scavenging activity by antioxidants establishes a homeostatic system. The imbalance disrupted by impaired ROS-scavenging antioxidants causes oxidative stress.[106] Current researches focus on smart drug delivery systems (SDDSs), gene therapies, and anti-miRNAs and the exploration of ROS-scavenging agents with definitive functions to attack mitochondrial ROS.[21] The evidence of antioxidant supplements in clinical applications for atherosclerosis is still lacking, possibly because they may disorder the normal homeostasis.[107]

An in-vitro study on activated macrophages showed that folate conjugation with catalases and SODs exhibited high ROS scavenging properties.[108] Folate-conjugated catalases scavenged ≈78%

of hydrogen peroxides produced by lipopolysaccharide (LPS)-treated macrophages, whereas free catalases scavenged only ≈20% of hydrogen peroxides. Similarly, folate-conjugated SODs scavenged ≈51% of superoxide radicals produced by the activated macrophages, while free SODs had no effect on superoxide radicals.[108] However, more in-vivo studies are needed in order to further verify this potency. Recently, a number of researchers have developed SOD-mimetic nanoparticles, which are inorganic nanoparticles with SOD-like activities and possibly can prevail over many limitations of native enzymes. These enzyme-like nanoparticles are termed as "nanozymes".[109] One of the reported nanozymes showing great promise is cerium oxide (CeO_2), a novel artificial SOD, which has an ultra-small size ranging from 3 to 20 nm[110] and can be used as potent ROS scavenging agents to suppress excessive ROS production in the progression of atherosclerosis.

Wang et al.[111] developed an SOD-mimetic agent (Tempol) and a hydrogenperoxide-eliminating compound of phenylboronic acid pinacol ester that were covalently conjugated on *β*-cyclodextrin (*β*-CD) (TPCD NPs) (**Figure 2**A). These ROS-responsive nanoparticles could scavenge multiple ROS, such as hydrogen peroxide, hydroxyl radical, superoxide anion, and hypochlorite and effectively inhibit foam cell formation in macrophages and VSMCs by reducing Ox-LDL influx (Figure 2B,C). These TCPD NPs had spherical morphology with a hydrodynamic diameter of around 128 ± 1 nm (Figure 2D). An in-vivo study revealed that high-dose TPCD NPs resulted in the lowest plaque area compared with other treatments (Figure 2D). Moreover, TPCD NPs could stabilize the plaques that were indicated by less cholesterol crystals, a smaller necrotic core, thicker fibrous cap, and lower macrophages and MMP-9s.

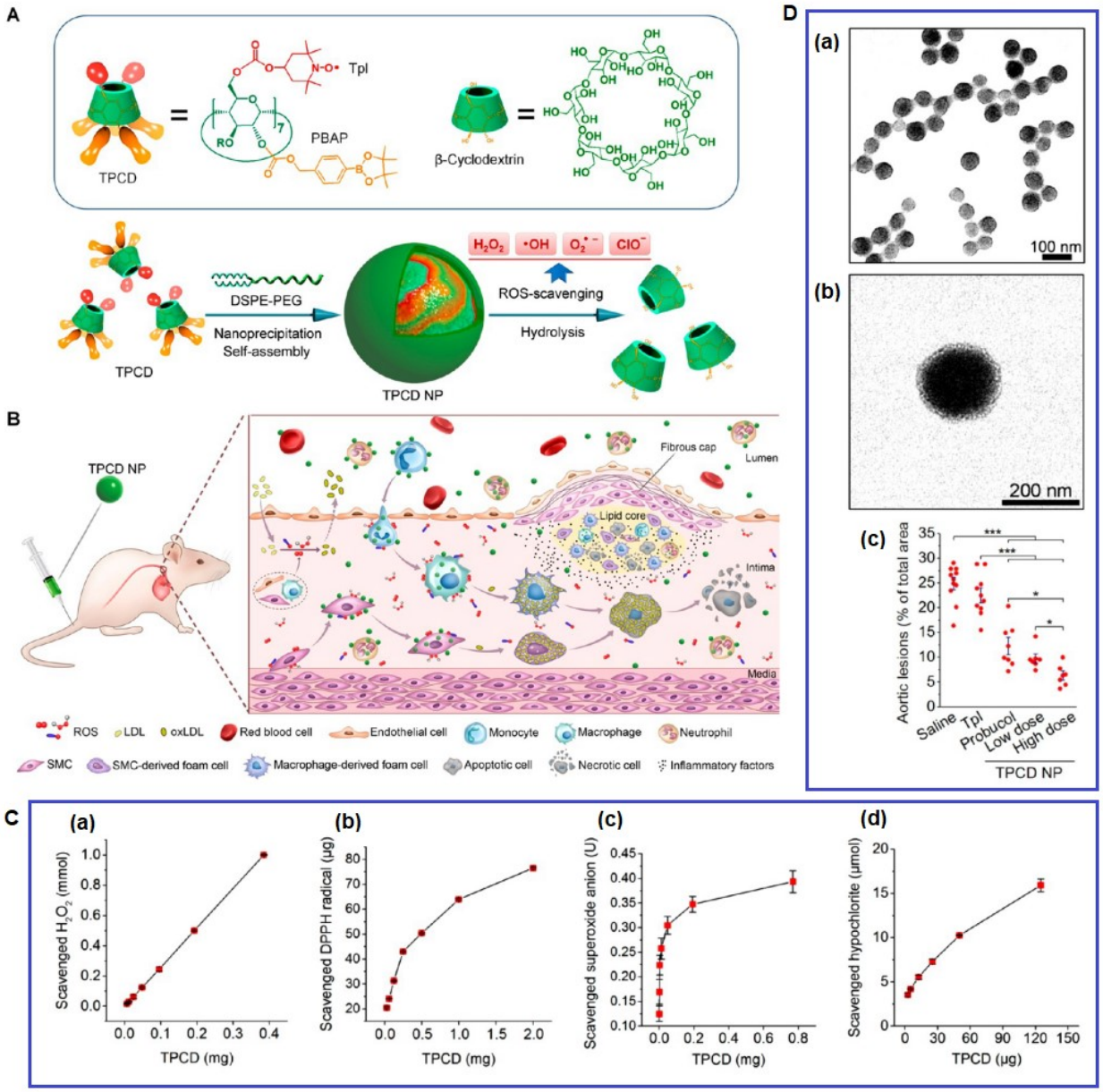

Figure 2. A) Chemical structure of a broad-spectrum ROS-eliminating material TPCD and development of a TPCD nanoparticle (TPCD NP). B) Sketch of targeted treatment of atherosclerosis by eliminating ROS through IV administration of engineered TPCD NP. C) Dose-dependent elimination of H_2O_2 (a), DHHP radical (b), superoxide anion (c), and hypochlorite (d) by TPCD. D) Transmission electron microscopy (TEM) image of TPCD NPs (a), TPCD NP after phosphotungstic acid staining (b), and quantitative analysis of the lesion area in aortas with different treatments (c). Adapted with permission.[111] Copyright 2018, American Chemical Society.

One of the effective strategies to attenuate lipid deposition and oxidation is the normalization of autophagy. Autophagy is a self-degradative system that plays a major role in the removal of protein aggregates, corrupt organelles such as mitochondria and endoplasmic reticulum (ER), and intracellular pathogens via lysosomes.[112] Current studies reveal that the autophagic system is impaired during the progression of atherosclerosis due to oxidative stress. Dysfunctional autophagy

is present mainly in macrophage- and vascular smooth muscle-derived foam cells in atherosclerosis.[113] To date, the number of works to normalize autophagy for atherosclerosis management via nanomedicine has shown significant outcomes.

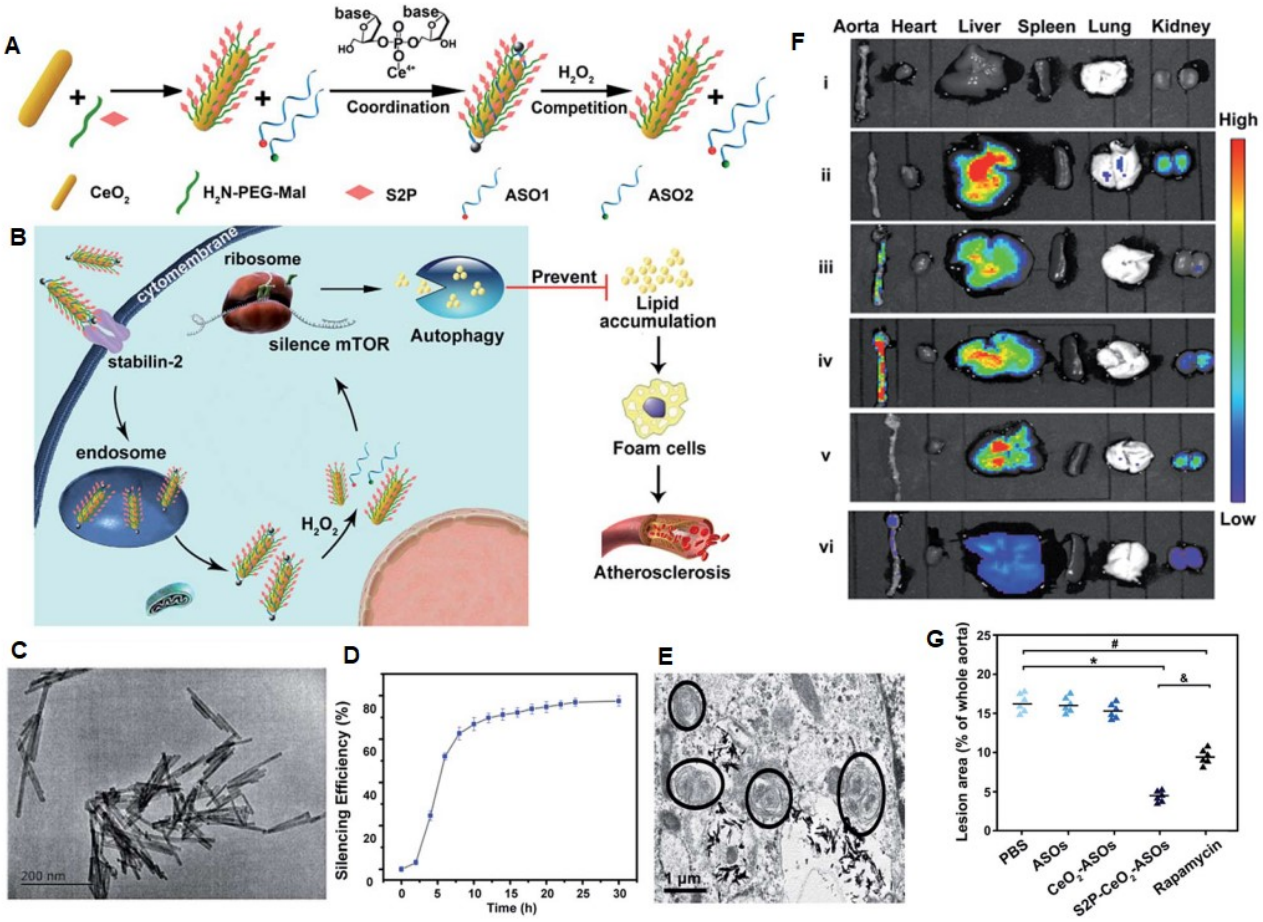

Figure 3. A) Molecular structure of the H_2O_2-responsive and plaque-penetrating nanoplatform, S2P-CeO_2-ASOs. B) Illustration of the S2P-CeO_2-ASOs nanoplatform for targeted mTOR gene silencing to attenuate atherosclerosis. C) TEM images of the S2P-CeO_2-ASOs nanoplatform incubated in PBS buffer (pH 7.4). D) Dependence of the mTOR silencing percentage upon incubation time after treating VSMCs with S2P-CeO_2-ASOs. E) Representative TEM images of autophagosomes after treatment with S2P-CeO_2-ASOs for 24 h. The black circles outline the double-membrane structures of the autophagosomes. F) Fluorescence images of the aortas and main organs of the plaque-bearing ApoE$^{-/-}$ mice sacrificed 24 h post-injection of (i) PBS, (ii) free ASOs, (iii) CeO_2-ASOs, (iv) S2P-CeO2-ASOs, (v) S2P peptide followed by S2P-CeO_2-ASOs and (vi) S2P-CeO_2-ASOs with H_2O_2 scavenger catalase. G) Quantification of the stained area as a percentage of the whole aorta with different treatments. Adapted under the terms of the CC BY 3.0 license.[114] Copyright 2018, the Royal Society of Chemistry.

Recently, Gao et al.[114] developed an active targeting-H_2O_2 sensitive nanoagent (S2P-CeO_2-ASOs) for the recovery of autophagic systems in apoptotic VSMCs and lipid-laden macrophages by silencing mammalian target of rapamycin (mTOR) with RNA interference (RNAi) oligonucleotides

(**Figure 3**B). This nanoagent used stabilin-2-specific peptide ligands (S2P) to improve the specificity of targeting and penetration, was PEGylated (modification using PEG) to prolong the blood circulation time, and utilized a CeO_2 core to facilitate endosomal escape and release the RNAi cargos in response to the hydrogen peroxide (H_2O_2) (Figure 3A). These CeO_2 nanowires had a hydrodynamic diameter of ≈100-150 nm (Figure 3C) and ≈90% of the loaded antisense oligonucleotides (ASOs) could be released within 5 min in the presence of 100 mM H_2O_2. These S2P-CeO_2-ASOs showed high accumulation in the aorta and liver (Figure 3F). An in-vivo study showed that the expression of mTOR in the aortas, a key regulator of autophagy,[115] could be reduced by more than 75% leading to a significant reduction of total plaque areas by ≈67.1% (Figure 3D,E,G). These results demonstrate that the acceleration of neutral lipid delivery to lysosomes and cholesterol removals from the foam cells can be achieved by blocking mTOR expression.[116]

Dou et al.[117] have successfully synthesized ROS-sensitive *β*-cyclodextrin (Ox-bCD) NPs for controlled drug release of RAP that could normalize autophagy. Cyclodextrins could effectively entrap diverse hydrophobic drugs due to the hydrophobic interior and hydrophilic exterior. In addition, drug release from the nanocarriers could be achieved via a ROS stimulus. These ROS-responsive nanoagents were delivered passively into the lesion sites via the leaky blood vessels and the lymphatic pathway mediated by translocation of neutrophils and monocytes by an intraperitoneal injection. This nanotherapy effectively inhibited the proliferation of macrophages and blocked the formation of foam cells, which showed positive effects on plaque stabilization and reduction in vivo (≈39.9% plaque reduction).

Another strategy to treat atherosclerosis is selective eradication of activated macrophages via photodynamic therapy (PDT). PDT uses photosensitizers that are nontoxic to cells in the absence of light irradiation and can be delivered into the plaques and activated after internalization by activated macrophages. PDT could generate ROS that can induce cell death in atherosclerotic plaques.[118] There are two different cell death pathways after photosensitization, namely non-programmed (necrosis) and programmed (apoptotic and autophagy) pathways. Generally, the apoptotic pathway

requires a low intensity of light irradiation, whereas the necrotic pathway needs a higher dose of light.[119]

Kim et al.[120] developed ROS-responsive theranostic nanoparticles (MacTNPs) targeting activated macrophages in atherosclerosis. These nanoagents were made of a Chlorin e6 (Ce6)-hyaluronic acid (HA) conjugate that was reactive to the presence of ROS, especially peroxynitrites. MacTNPs were irradiated with NIR light, but the activation of photosensitizers was still quenched by the HA coating. After internalization by the activated macrophages, the immoderate intracellular ROS, especially peroxynitrites, broke down the shells of MacTNPs by cleaving the chemical bonds of HA and released the photosensitizers. As a result, it generated near-infrared (NIR) fluorescence emission and singlet oxygen. Light irradiation (10 J cm^{-2}) induced the necrosis in ≈66% of the activated Raw 264.7 cells but not in human dermal fibroblast cells. However, PDT-mediated autophagy is preferred over non-programmed cell death. PDT treatment could suppress the number of proliferative macrophages and thus increase the stability of plaques.

3.1.2. Enzyme Responsive

A significant number of enzymes are actively involved in the progression of atherosclerosis, such as MMPs, hyaluronidases, and cathepsins. MMPs are a class of proteolytic enzymes that degrade ECM proteins such as collagen (by MMP-1s, MMP-8s, and MMP-13s), gelatin (by MMP-2s and MMP-9s), elastin (by MMP-12s), and fibrin (by MMP-3s and MMP-10s).[118] Hyaluronidases are a class of enzymes that primarily degrade HA. Hyaluronidases have absolute specificity for HA,[122] a non-collagen component of the ECM, which plays a prominent role in the response of tissues to injury.[123] In addition, cathepsins are a class of proteolytic enzymes that are particularly present in lysosomes. After the release from macrophages, cathepsins can enhance the inflammatory activity of atherosclerosis. Cathepsin B breaks down the ECM within the tunica intima, together with cathepsin D and X, leading to a thin fibrous cap, which is the main characteristic of plaque vulnerability.[124]

Recently, those enzymes have become attractive stimuli and targets for drug delivery and imaging of atherosclerosis as they play a key role in the progression of plaque instability.

There are three major targets of MMP-SRNAGs, namely MMP-13s, MMP-2s, and MMP-9s. MMP-13s have been known to prevail over MMP-8s as a prominent interstitial collagenase in mouse atheromata.[125] A number of cells can produce MMP-13s, but macrophages are the main MMP-13 initiators in human atherosclerotic plaques.[126] Recently, many classes of MMP-13 inhibitors have been developed to inhibit MMP-13 activities. Radiolabeled MMP-13 inhibitors, for instance, have been investigated as tracers for the detection of activated MMP-13s using PET. Those MMP-13 inhibitors were made of an *N,N'*-bis(benzyl)pyrimidine-4,6-dicarboxamide core and radiolabeled with carbon-11 (^{11}C), fluorine-18 (^{18}F), and gallium-68 (^{68}Ga) and could selectively obstruct MMP-13 activity with no significant number of tracers remaining in non-excreting organs 60 min, 90 min, and 90 min post-injection for ^{11}C, ^{18}F, and ^{68}Ga radiotracers, respectively.[127]

Quillard et al.[128] developed ION-based-MMP-13 inhibitors (MMP13i-A agents). The fluorescence emission of the MMP13i-A agents was quenched during the delivery in the bloodstream and only activated when the nanoagents were cleaved by MMP-13s in the plaque lesions. The MMP13i-A agents attenuated MMP-13 activities by ≈76% and ≈53% in activated murine- and human-macrophages, respectively. Ex vivo quantification using fluorescence reflectance imaging (FRI) showed that there were a 407% rise in MMP-13 signals and a 344% rise in macrophage phagocytic activities in the arteries of the atherosclerotic mice. This inhibition resulted in thicker fibrous caps due to elevated collagen contents in the atherosclerotic plaques.

The degradation of ECM by MMPs results in destabilization of atherosclerotic plaques, which may have a positive correlation with rupture-prone plaques.[129-133] Gelatinases (MMP-2s and MMP-9s) are the predominant MMPs secreted by T-lymphocytes and macrophages.[134,135] Recent researches reported that MMP-9s and MMP-2s were highly present in macrophage- and VSMC-rich lesions, respectively.[136,137] A number of MMP-2 and MMP-9 inhibitors have been developed over the last decade. Firstly, novel radiotracers based on *N*-benzenesulfonyliminodiacetyl monohydroxamates and

N-halophenoxy-benzenesulfonyl iminodiacetyl monohydroxamates were developed with high selectivity and obstructive potential towards MMP-2s and MMP-9s. Moreover, these MMP-2/MMP-9 inhibitors could be visualized using SPECT. Iodine-123 (^{123}I) radiolabelling showed the highest obstructive potency and selectivity for both MMP-2s and MMP-9s.[138] Secondly, gold nanorods conjugated with MMP-2 antibodies (AuNRs-Abs) were effectively used as hybrid PAI agents for the quantitative detection of MMP-2s in atherosclerotic plaques.[139] Lastly, a fluorine-18-labeled MMP-2/MMP-9 inhibitor (^{18}F-1) and a tritiated selective MMP-9 inhibitor (^{3}H-2) were used as PET imaging agents. In vitro autoradiography showed that both inhibitors bound to stable and vulnerable atherosclerotic plaques. The ^{3}H-2 inhibitors showed twofold higher accumulation in atherosclerotic lesions than in healthy tissues.[140]

Apart from MMPs as targeted enzymes, hyaluronidases also serve as important targets for drug delivery to atherosclerotic plaques as they can specifically degrade HA (an important biopolymer that is usually used for surface coating of nanocarriers). There are two main receptors of HA that are overexpressed in atherosclerotic lesions, namely CD44 and stabilin-2 (HARE). CD44 has been found to be overexpressed not only in rupture-prone plaques (tenfold more than in normal tissues),[141-144] but also on the surface of endothelial cells, macrophages and VSMCs in atherosclerotic lesions.[142,143,145] Silencing CD44 in ApoE$^{-/-}$ mice can reduce the plaque formation by >50%.[142] Furthermore, compared to healthy vessels, HARE is overexpressed in atherosclerotic lesions and on the surface of macrophages, VSMCs, and endothelial cells in the plaques.[146] Therefore, CD44 and HARE can be used as active targets for drug delivery in atherosclerosis by using HA-coated NPs to enhance the nanoparticle uptake and HA degradation by hyaluronidases in the interstitial fluid (under the fibrous cap).

Recently, HA-coated reconstituted high-density lipoprotein (r-HDL) NPs have become one of the most promising nanoagents for atherosclerosis management due to their multiple potencies for RCT and delivery of statins.[147,148] HDL is known as good cholesterol because it can remove excessive cholesterol from atherosclerotic plaques and deliver it back to the liver. Moreover, it shows anti-

inflammatory and antioxidative potencies that safeguard the cardiovascular system. HDL removes excessive cholesterol from macrophage-derived foam cells in atherosclerotic lesions via RCT.[149] Due to the limited production of endogenous HDL in the liver and the complicated steps and cost to isolate and purify the native HDL from human plasma under current good manufacturing practice (cGMP),[150] various r-HDL NPs have thus been widely investigated recently.

The major problem in the delivery of r-HDL NPs into atherosclerosis lesions is undesirable accumulation in the liver due to high expression of scavenger receptor class B type I (SR-BI) not only in activated macrophages but also in hepatocytes.[150,151] Coating r-HDL NPs with HA can prolong the circulation time of nanoagents in the bloodstream and enhance the accumulation of nanoagents in atherosclerotic lesions by actively targeting CD44 and HARE receptors. After degradation of HA coating by hyaluronidases, naked r-HDL NPs will be internalized by macrophage-derived foam cells via SR-BI receptor-mediated endocytosis.[147-150] An in-vivo study showed that r-HDL NPs could lessen total cholesterol, low-density lipoprotein cholesterol (LDL-C), and triglyceride levels, raise the high-density lipoprotein cholesterol (HDL-C) levels,[147] and reduce plaque size.[150]

Recently, HA coating has also been used for gene delivery to downregulate the overexpression of LOX-1, which is a receptor of Ox-LDL in macrophages that plays a key role in cholesterol influx. The HA coating promotes nanoagents to accumulate at the leaky endothelium by specific binding to CD44 receptors. The nanoagents (HA-coated CPPs/siRNA NPs) could then be broken down by hyaluronidases to release bare cell penetrating peptide (CPP)-nanocomplexes that facilitate the internalization of nanocomplexes into macrophages via a caveolae-mediated endocytosis pathway (**Figure 4**A). The hydrodynamic diameter and zeta potential of these nanocomplexes were around 140-153 nm and (-22)-(-30) mV, respectively (Figure 4B,C). High coating density of HA with large molecular weight on nanocomplexes (NPs-3) showed high accumulation in the aorta and liver (Figure 4D) and exhibited the most significant effects on the reduction of plaque sizes and lipid deposition, macrophage infiltration, and monocyte chemoattractant protein-1 (MCP-1) expressions.[152]

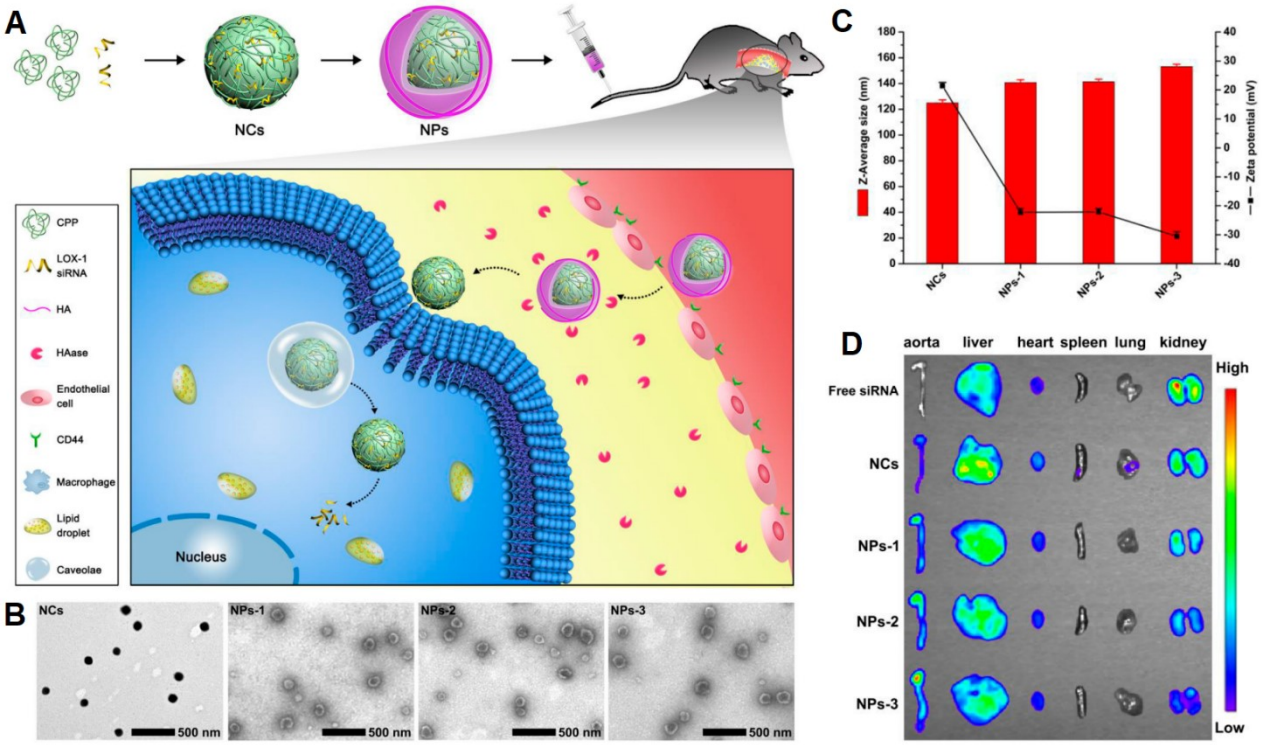

Figure 4. A) Illustration of HA-coated CPPs/siRNA nanoparticles for targeted gene delivery to macrophages in atherosclerotic plaques. B) TEM images of different formulations. C) Particle size and zeta potential of CPPs/siRNA nanocomplexes (NCs), HA (M_w 8 kDa)-coated NCs (NPs-1), HA (M_w 200 kDa, low coating density)-coated NCs (NPs-2), and HA (M_w 200 kDa, high coating density)-coated NCs (NPs-3). D) H&E histopathological sections of vital tissues, including heart, liver, spleen, lung, and kidney, after treatment with various preparations. Adapted with permission.[152] Copyright 2018, American Chemical Society.

As mentioned before, cathepsin B is a protease secreted by macrophages that plays a major role in ECM degradation together with MMPs. In unstable plaques, cathepsin B activity is significantly higher than in stable plaques.[153] Therefore, it can serve as both a stimulus and a target for drug delivery in atherosclerosis management. Shon et al.[154] developed protease-mediated theranostic agents (L-SR15 agents) for PDT that could suppress cathepsin B activity. L-SR15 activation was mediated by cathepsin Bs that released Ce6 molecules leading to the reduction of foam cells via PDT.[155-157] This photosensitizer (Ce6) could be used for PDT and fluorescence imaging. A similar finding was reported by Kim et al.[158] who developed cathepsin B-activatable NIR fluorescent imaging agents to examine the therapeutic effects of atorvastatin and glucosamine on mouse atheromata. The fluorochromes were dequenched and emitted fluorescent light after exposure to cathepsin Bs. High-dose glucosamine could suppress cathepsin B activity and promote plaque stabilization.

3.1.3. pH Responsive

It has been well known that the extracellular fluid in inflammatory sites is acidic.[159] The hypoxic condition of atherosclerotic lesions enhances the lactate concentration due to the accumulation of activated macrophages that actively engulf Ox-LDL with an extremely high energy demand, which forces macrophages to use anaerobic glycolysis for ATP production.[160,161] The uncontrolled amount of lactate is secreted by macrophages through the work of chemical pumps, transporters, and exchangers, which results in a drop of the pH of the interstitial fluid in atherosclerosis lesions.[162] Furthermore, Naghavi et al.[163] used two pH-sensitive fluorescent dyes to assess the pH values of atherosclerotic plaques in vivo. The results indicated that the ranges of pH were around 6.5 to 8.5 and 5.5 to 7.5 in human and rabbit atherosclerotic lesions, respectively. More importantly, it is well known that lysosomes are acidic, which indicate a pH range of about 4.7 to 4.8 in macrophages.[164] The slightly acidic interstitial fluid (pH around 6.0 to 6.8) in atherosclerotic lesions[163] and the acidic lysosomal condition (pH below 5.0) in macrophages[164] can be used to control drug release for atherosclerosis management.

To date, only a few studies have been carried out on the design of pH-responsive nanoagents for controlling drug release and imaging applications in atherosclerosis management. Nonetheless, these studies have shown great promise in designing pH-sensitive theranostic nanoagents for drug, antioxidant, and gene delivery to treat atherosclerosis. Tang et al.[165] developed pH-responsive multifunctional nanoparticles based on encapsulated tannic acid (TA) and imaging agents in PEG polymer directed self-assembly using flash nanoprecipitation. These nanocomplexes (TA NPs) acted as natural scavengers of ROS for atherosclerosis treatment. At pH 7.4, TA NPs had a homogeneous solid spherical core containing encapsulated iron within a block copolymer shell. However, at pH 5, TA NPs were swollen and became porous due to solubilization of a portion of the TA-iron complex. The stability constant of TA-iron bis-complex at pH 5 was $\approx 10^9$ compared with $\approx 10^{17}$ for the tris-complex,[166] possibly affecting dismantlement and recast of nanoparticles. More importantly, due to

the acidic microenvironment of lysosomes, the stabilized tris-complex of TA and Fe^{3+} at pH below 5 shifted to less stabilized bis-complex and released TA in the lysosomes, possibly creating a pathway for intracellular conveyance of antioxidants. Owing to the antioxidant properties of TA,[167] these TA NPs have low cytotoxicity and high ROS scavenging activity.

Park et al.[168] developed doxorubicin-loaded hyaluronic acid-polypyrrole nanoparticles (DOX@HA-PPyNPs) as an intelligent theranostic nanoagent to treat proliferating macrophages in plaque lesions. These PPyNPs exhibited great potential as ultra-efficient energy quenchers as they could extinguish DOX fluorescence when DOX molecules were placed near the PPyNP surface due to the effective energy transfer from DOX to PPyNPs. In the extracellular fluid, where the pH was ≈7.4, the carboxylic acid clusters of HA were negatively charged and the charge block between DOX and HA-PPyNPs was relatively constant, so the DOX fluorescence remained inactive in the blood circulation. However, after the accumulation of DOX@HA-PPyNPs at the targeted lesions, followed by internalization by proliferating macrophages, the DOX fluorescence was activated under acidic lysosomal conditions. DOX released from nanocarriers was provoked by the forfeit of the negative charges of HA in low pH. An in-vitro study showed that ≈57% of drugs were released at pH 5.0 over 8 h, and the amount of released DOX reached nearly 100% after 24 h. In addition, ≈60% of the proliferating macrophages became apoptotic after 0.5 mM DOX treatment.

Recently, Dou et al.[117] developed acetalated β-CD (Ac-bCD) NPs for controlled drug release of RAP, a specific mTOR inhibitor, using the acidic pH level as an endogenous trigger for atherosclerosis treatment (**Figure 5**). Drug release from the nanocarriers could be achieved by the mildly acidic microenvironment in the progression of atherosclerosis. These Ac-bCD NPs had a hydrodynamic diameter of ≈187 nm and were delivered passively into the lesion sites. This nanotherapy effectively suppressed the proliferation of macrophages and blocked the formation of foam cells. Interestingly, ≈97.2% of drugs were released from nanocarriers at pH 5.0 within the first 2 h. The mice study showed that RAP nanotherapies based on Ac-bCD NPs reduced the average plaque area by ≈35.0% after therapy.

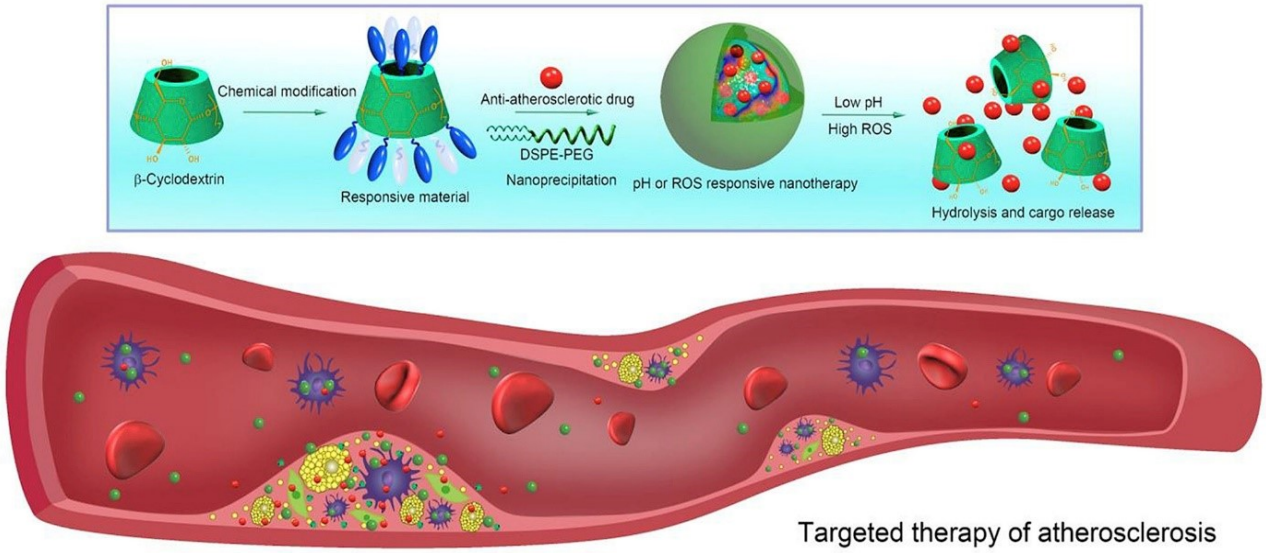

Figure 5. Schematic representative of an acid-labile material of acetalated *β*-CD (Ac-bCD) and a ROS-sensitive *β*-CD material (Ox-bCD) for atherosclerosis treatment. Reproduced with permission.[117] Copyright 2017, Elsevier.

Gupta et al.[169] developed oligoproline peptide-derived nanocarriers for plasmid DNA (pDNA) delivery targeting VSMCs in plaque lesions. The nanocarriers were made of a pH-responsive (PPDDBP) polymer consisting of a P(DMAEMA-*co*-BMA-*co*-PAA) core-stabilizing block and PEG coating to efficiently entrap plasmid DNAs. The PPDDBP/pDNA polyplexes were stable and formed globular shapes with an average hydrodynamic diameter of 120 nm in DPBS (pH 7.4). These nanoagents were programmed to firstly interact with ROS in the interstitial fluid, which mediated dePEGylation of polyplexes and then initiated cellular uptake in VSMCs through the interaction of positively charged PDMAEMA with the negatively charged plasma membrane of VSMCs. Finally, intracellular acidic endosomal conditions promoted the destabilization of the second layer of nanocarriers and membrane disorganization leading to endosomal escape and increased pDNA transfection efficiency. More than 90% of human coronary artery smooth muscle cells were alive with N/P ratio under 10, suggesting that PPDDBP/pDNA polyplexes had higher cytocompatibility.

3.1.4. Shear-Stress Responsive

It is noteworthy that blood vessels are continuously exposed to diverse kinds of hemodynamic forces, such as fluid shear stress, hydrostatic stress, and cyclic stretch initiated by the pulsatory blood stress and stream.[170] The narrowing of blood vessels, which results from atherosclerosis progression, promotes the elevated hemodynamic fluid shear stress or wall shear stress (WSS) at the sites of atherosclerosis. The range of WSS in vulnerable plaques was predicted to be between 31.90 and 136.09 dyn cm^{-2},[171] whereas WSS in normal vessels was generally around 1-10 dyn cm^{-2}.[172] In addition, WSS is much higher in the proximal region (180 dyn cm^{-2}) than in the distal region (100 dyn cm^{-2}).[173] This abnormal shear stress can be used as a stimulus to trigger drug release and local delivery of drugs to the sites of vulnerable plaques (constricted vessels). So far, most of the micro and nanoparticle designs for shear-mediated drug delivery are subjected to mimic platelets that play a key role in atherothrombosis and vascular injury. These methods take advantage of the binding of fibrinogen, vWF, and fibronectin to the activated integrin $\alpha_{IIb}\beta_3$ under elevated shear stress and thereby promote platelet aggregations for the treatment of vessel clots.[174,175]

The high shear stress in atherosclerosis open new opportunities for the development of shear-stress-responsive nanoagents for atherosclerosis management. To date, only limited reports utilize the high shear-stress stimulus for local drug delivery to vulnerable plaque sites to prevent plaque instabilities. Holme et al.[176] developed shear-stress-sensitive lenticular vesicles for targeted drug delivery to vulnerable atherosclerotic plaques (**Figure 6**). These nanovesicles, Pad-PC-Pad $LUVET_{100}$ with a maximum hydrodynamic diameter of 114 nm, were based on artificial 1,3-diaminophospholipids that were stable under static conditions but labile at elevated shear stress due to their lenticular morphologies, so the drugs could easily be released in the locations with high shear stress (Figure 6A). More than 95% of cargos (carboxyfluorescein fluorophores) were successfully released from Pad-PC-Pad nanovesicles when passing through a constricted artery, a vulnerable-plaque model, with shear stress at ≈50 dyn cm^{-2} (Figure 6B-D).

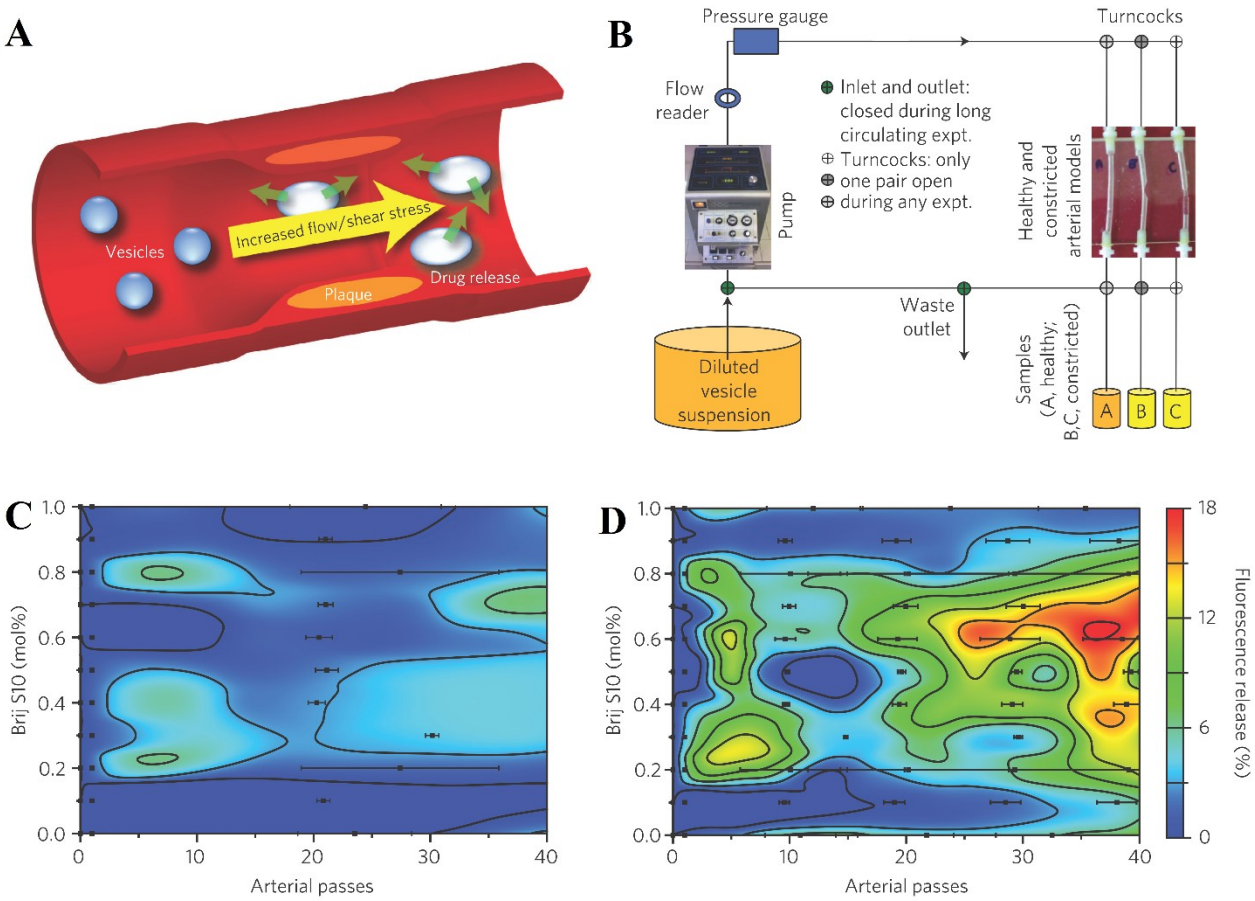

Figure 6. Release of entrapped fluorescent dye after passage through an extracorporeal pump flow set-up. A) Schematic of the hypothesis using changes in endogenous shear stresses as a physical trigger for drug delivery. B) Experimental set-up. An extracorporeal heart pump is connected to a plastic model of healthy or constricted arteries. The system is closed once the product is loaded and the vesicles are allowed to circulate in the system for 20 min. C,D) Fluorescence release patterns of EggPC vesicles with 0-1 mol% Brij S10 at 37 °C. C) Release in the healthy artery model and D) release in the constricted artery model. Brij S10 concentration is plotted against number of passes through the artery model, with fluorescence release along the z-axis. Background fluorescence release is subtracted for each set. Reproduced with permission.[176] Copyright 2012, Springer Nature.

3.2. Exogenous Stimuli-Responsive Nanoagents

3.2.1. Light Responsive

Nowadays, the development of light-responsive nanoagents is expanded not only for imaging purposes, but also for therapeutics, especially using fluorescence imaging techniques. In comparison with fluorescence imaging in the visible light zone (400-700 nm), fluorescence imaging in the NIR region (700-1700 nm) offers a lot of benefits and enables better imaging resolution, higher signal-to-noise ratio, and deeper tissue penetration.[177] More importantly, NIR-fluorophores, especially in NIR-II zone (1000-1700 nm), can convert NIR-photons into heat that is useful for photothermal

therapy (PTT) and be stimulated by NIR light to generate singlet oxygen for PDT.[178] Therefore, those NIR-based fluorophores both from organic and inorganic compounds have drawn much attention in the development of SRNAGs for atherosclerosis management.

The therapeutic effects of PTT markedly rely upon the capability of photoabsorbers to transform light into sufficient heat. PTT utilizes photothermal agents to generate heat, which results in the elimination of unwanted cells upon NIR laser irradiation.[178-180] In clinical trials, nano-intervention by silica-gold iron-bearing nanoparticles with targeted microbubbles and magnetic navigation for NIR-mediated PTT successfully reduced the total atheroma volume and plaque burden by ≈47.9 mm^3 and ≈39.4%, respectively.[181] More recently, Gao et al.[182] developed copper sulfide nanoparticles coupled with antibodies, with a particle size of ≈13 ± 1.2 nm (**Figure 7**B), targeting transient receptor potential cation channel subfamily V member 1 (TRPV1) as a photothermal switch in VSMCs mediated by NIR light. After 30-s NIR light exposure (980 nm, 5 W cm^{-2}), the temperature notably increased from 37 °C to 42.7 °C in the VSMCs incubated with CuS-TRPV1, which was sufficient to activate TRPV1 channels and produce robust photoacoustic signals for PAI (Figure 7C). More importantly, the elevated temperature could open thermo-sensitive TRPV1 gates leading to the Ca^{2+} influx (Figure 7A). This increased intracellular Ca^{2+} concentrations could reactivate the autophagic system and eventually suppress foam cell formation through the AMP-activated protein kinase (AMPK) signaling pathway. An in-vivo study in $ApoE^{-/-}$ mice showed that there were 54.2% and 72.3% reductions in aortic root lesion sites and in aortic arch lesion sites, respectively (Figure 7D-F).

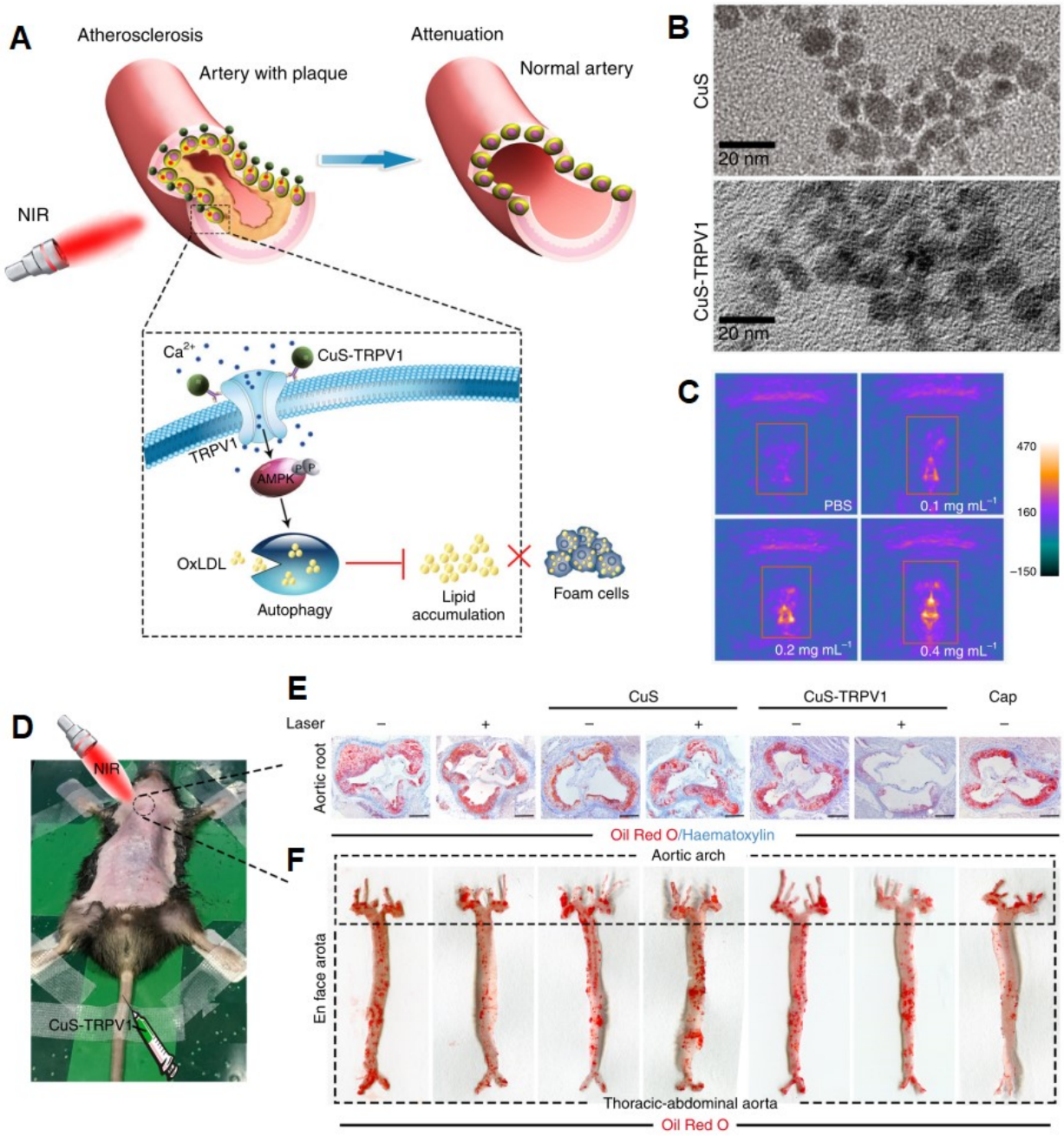

Figure 7. A) Illustration of CuS-TRPV1 switch for photothermal activation of TRPV1 signaling to attenuate atherosclerosis. B) TEM images of CuS and CuS-TRPV1. Scale bar = 20 nm. C) PAI of CuS-TRPV1 dispersed in PBS buffers with different concentrations (0, 0.1, 0.2, and 0.4 mg mL^{-1}). D) NIR laser treatment. E) Representative images of Oil Red O-stained aortic root sections. Haematoxylin was used as a counterstain. Scale bar = 250 μm. F) Representative images of Oil Red O-stained en face aortic preparations. Within the dashed box above is the aortic arch and below it is the thoracic-abdominal aorta. Adapted under the terms of the CC BY 4.0 license.[182] Copyright 2018, Springer Nature.

Another therapy using NIR-fluorophores is PDT. In recent years, a number of researchers have demonstrated the efficacy of PDT for atherosclerosis treatment. There are three major elements in the PDT system, namely light, photosensitizers, and oxygen. The photosensitizers can generate ROS, such as singlet oxygen, free radicals or peroxides, under the stimulation of a suitable light

wavelength,[176] which can induce cell death and facilitate plaque stabilization. After photosensitization, non-programmed (necrosis) and programmed (apoptotic and autophagy) cell death pathways can be achieved via high and low intensities of light irradiation, respectively.[119]

Recently, Han et al.[183] developed mesoporous silica-coated upconversion fluorescent NPs encapsulating chlorin e6 (UCNPs-Ce6) for PDT. The effects of PDT could effectively induced programmed cell death of THP-1 macrophages via the PI3K/Akt/mTOR signaling pathway and enhanced cholesterol efflux from the macrophages. Higher UCNPs-Ce6 concentrations and longer duration of laser illumination led to lower cell viability with the optimal setting at the concentration of 8 μg mL^{-1} and light intensity of 1.0 W cm^{-2} for 60 s. Moreover, the upconversion nanoparticles (UCNPs) could switch NIR light to visible light, which was beneficial for noninvasive imaging, although the image quality of NIR-NIR imaging is better than NIR-visible imaging.[184] Similarly, Yi et al.[185] developed light-sensitive theranostic nanoagents (Ce6/DS-DOCA) targeting SR-A receptors for depleting activated macrophages in atherosclerotic lesions (**Figure 8**A). The designed nanoagents were excellently internalized by lipopolysaccharide (LPS)-activated RAW 264.7 cells mediated by SR-A receptors. More than 75% of cells were eliminated by producing highly reactive singlet oxygen under 980-nm laser illumination (Figure 8B).

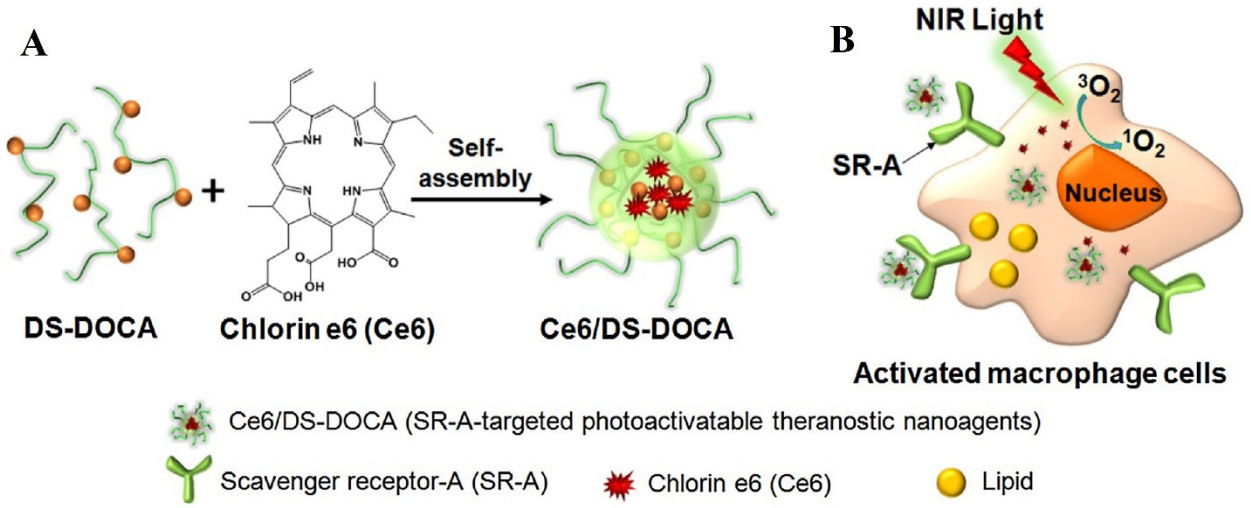

Figure 8. A) Preparation procedures of SR-A-targeted photoactivatable theranostic nanoagents. The theranostic nanoagents were prepared by the loading of Ce6 into dextran sulfate-deoxycholic acid (DS-DOCA) nanoparticles (delivery system) via hydrophobic interactions. B) PDT effects of SR-A targetable and photoactivatable theranostic Ce6/DS-DOCA nanoagents on activated macrophages. Under light irradiation, intracellularly delivered Ce6/DS-DOCA generated a highly reactive singlet oxygen that caused the apoptosis of activated macrophages. Reproduced with permission.[185] Copyright 2017, Elsevier.

In addition, NIR-fluorophores conjugated with nanocarriers can also be used as potent fluorescent imaging probes, thereby facilitating theranostic nanomedicine for atherosclerosis management. For instance, indocyanine green (ICG), a Food and Drug Administration (FDA)-approved organic fluorescent dye,[186] has been widely used as a fluorescent imaging agent. Moreover, ICG also has the capability as a photothermal agent for PTT[187,188] and a photosensitizer for PDT.[188,189] Very recently, Ma et al.[190] developed human serum albumin (HSA)-based theranostic nanoagents (ICG/SRT@HSA-pept NMs) encapsulating ICG and sirtuin 1 (Sirt1) activator SRT1720 with peptide moiety targeting osteopontin (OPN) ligands. These nanoagents could activate the intracellular Sirt1 and exhibit anti-atherosclerotic effects by blocking the VSMC-phenotype transition. In vivo evaluation in high-fat diet mice showed that PDT-mediated ICG/SRT@HSA-peptNMs enhanced therapeutic benefits, inducing better plaque reduction with a preferable necrotic core and thicker collagen compositions to restrain the plaque progression.

Furthermore, ICG could also be used for light-triggered drug release when loaded into liposomes (ICG-liposomes) as shown by Lajunen et al.[191] who developed ICG as a sensitive drug release system for non-cancer targeted sites. ICG stability can be dramatically modified via micellar encapsulating systems.[192] By loading ICG into phospholipids, self-quenching of the dyes can be attenuated, thereby enhancing the fluorescence intensities compared to the free compounds.[193] The ICG-liposomes could load small and large drug molecules, represented by calcein and FITC-Dextran 20 kDa. After exposure to an 808-nm 3-W laser source for 15 s, approximately 90% of calcein or Dextran was released from the liposomes with an ICG/lipid molar ratio of 1:50. These ICG-liposomes have shown great potential for light-responsive controlled release of small and large drug molecules enabling both slow and fast release (depending on the light dose) to treat macrophages,[191] which serve as an important target for many diseases, especially atherosclerosis.

3.2.2. Ultrasound Responsive

Ultrasound imaging has a number of benefits such as low-cost, non-invasive, real-time, high tissue contrast, and safe (no radiation) properties.[194] The application of Contrast-Enhanced Ultrasound (CEUS) Imaging using contrast agents started in 1968,[195] and it took over two decades to invent AlbunexR, the first generation of microbubbles, which was approved by FDA to enhance the imaging quality of ultrasonography. Since then, the stability and biocompatibility of ultrasound contrast agents have been continuously improved and microbubbles have been modified with ligands or antibodies for specific and active targeting of certain diseases.[195] Now, the applications of CEUS imaging are widely expanded for molecular imaging, which started around 2000, and drug delivery, which started around 2005. The use of microbubbles as carriers and the controlled release profiles are achieved by sonoporation,[196,197] referring to the formation of small pores (nanobubbles) after microbubble burst upon exposure to high acoustic power to release and deliver drugs or genes to targeted tissues.

Due to its safety profile, many microbubble-based ultrasound contrast agents have been approved by the FDA and they are now commercially available in the market such as Optison, Definity/Luminity, Sonovue/Lumason, and Sonazoid.[198] Recently, microbubbles have largely been exploited for theranostic nanomedicine in tumor and cardiovascular diseases. Much effort has been devoted to reduce the diameter of microbubbles to nanometer sizes for enabling both EPR-mediated extravasation and increasing nanoparticle uptake via active targeting. Current strategies that help deliver microbubbles to atherosclerotic plaques include platelet- and leukocyte-mimicking, and active targeting with ligands or antibodies, whereas nanobubbles can be delivered via active and passive targeting mechanisms.

It is noteworthy that shear stress in vulnerable plaques varies from 52.70 dyn cm^{-2} to 92.94 dyn cm^{-2}[171] and triggers platelet activation,[199] adhesion, and aggregation[174] at the advanced atherosclerotic sites. The interaction of platelet glycoprotein Ib (GPIb) and activated von Willebrand factor (vWF) on inflamed vascular endothelial cells is beneficial for promoting the attachment of platelet-mimicking microbubbles on the surfaces of constricted vessels by “catch-bond” kinetics.[200]

This characteristic was used by Owen et al.[201] to develop microbubble contrast agents for molecular imaging of unstable plaques. Microbubbles bearing GPIb showed a tenfold greater attachment to vWF than control microbubbles in a parallel-plate flow chamber. By molecular imaging using CEUS, the signal enhancement for vWF-targeted microbubbles was approximately fourfold greater in LDLR$^{-/-}$/ApoBec-1$^{-/-}$ mice than in wild-type mice.

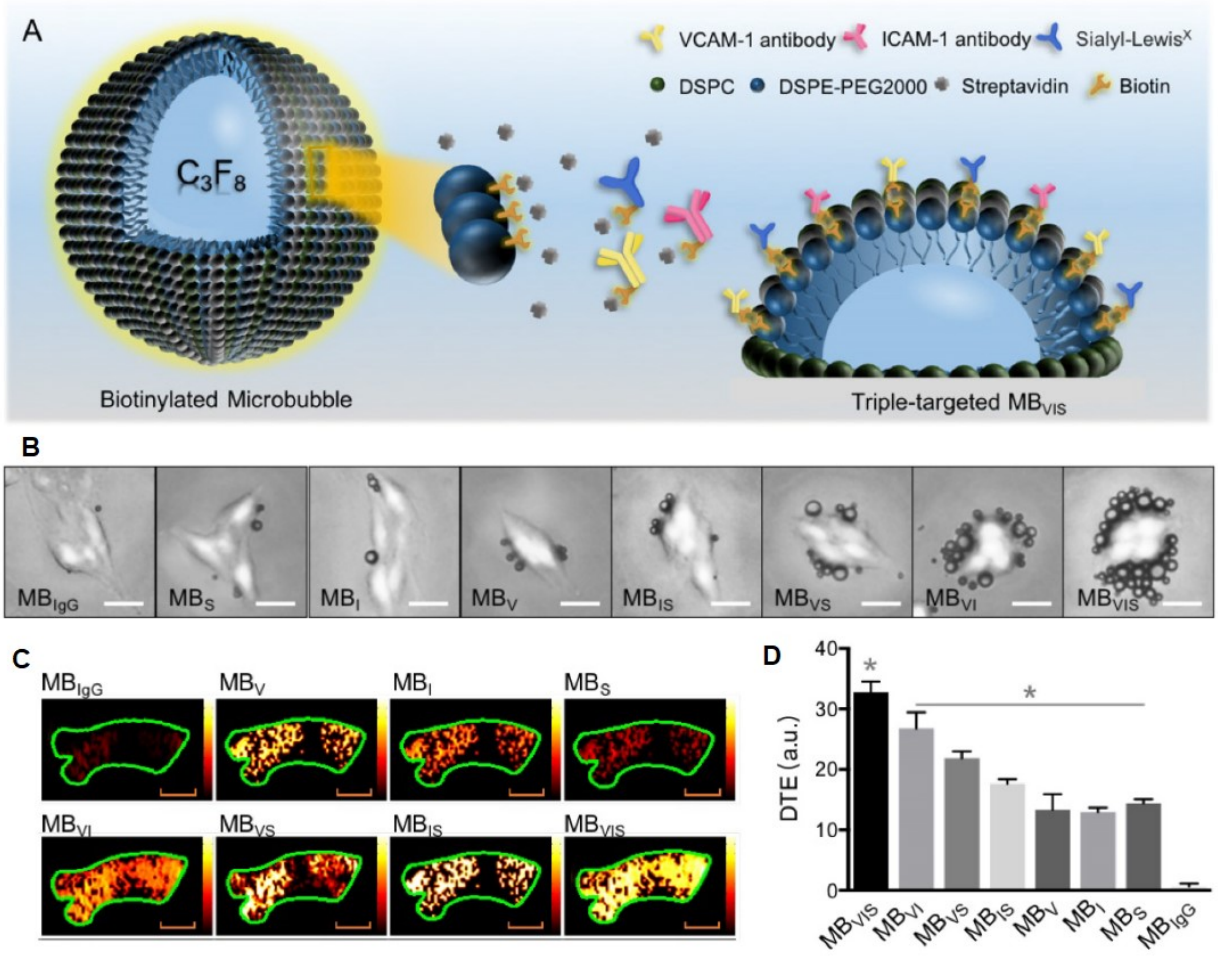

Figure 9. A) Schematic diagram of targeted MB_{VIS}. B) Representative bright-field micrographs of targeted MBs and MBIgG bound to stimulated bEnd.3 cells. C) Representative color-coded ultrasound images after injection of various kinds of MBs at the 10 week feeding time. D) Quantitative analysis of ultrasound signal intensities. Adapted under the terms of the CC BY-NC 4.0 license.[202] Copyright 2018, Ivyspring International Publisher.

Recently, Yan et al.[202] designed microbubbles for molecular imaging to evaluate the effects of atorvastatin therapy in atherosclerosis. The microbubbles were designed with leukocyte-mimicking properties using a triple-targeting strategy by integrating VCAM-1 and ICAM-1 antibodies and synthetic polymeric sialyl Lewis X (sLex) onto the microbubble surface, termed as MB_{VIS} (**Figure**

9A). A biotin-avidin linkage was used to conjugate the antibody ligands with the microbubble surface (DSPE-PEG_{2000}). The sLex binding with selectins mediated MB_{VIS} adhesion and ICAM-1 antibodies mediate slow rolling, while VCAM-1 antibodies arrested the MB_{VIS}. In the parallel-plate flow chamber experiment, MB_{VIS} exhibited more than twofold higher cell-binding strength within a minute compared with single-/dual-targeted microbubbles (Figure 9B). MB_{VIS} also exhibited the strongest signal intensity, giving contrast images for CEUS imaging (Figure 9C,D). After an 8-week evaluation, atorvastatin intervention effectively suppressed atherosclerosis progression with remarkably dropped ultrasound signals in the drug-treated A-HD mice ($ApoE^{-/-}$ mice fed with hypercholesterolemic diet) than in the control groups.

Microbubbles can also be designed for theranostic nanomedicine, enabling simultaneous diagnosis and therapy. Zhang et al.[203] designed simvastatin-loaded polymeric microbubbles (S-MBs) that promised faster drug release upon exposure to high acoustic power ultrasound. By conjugation with anti-ICAM-1 antibodies on the surfaces of S-MBs, the specific targeting of S-MBs to the dysfunctional endothelium at the atherosclerotic lesions was improved. After the internalization of S-MBs, high acoustic power ultrasound could trigger the release of ≈44% of simvastatin from microbubbles within 2 min, while no exposure to ultrasound only counted ≈12% of drug release. Furthermore, CEUS images using S-MBs showed a stronger echo intensity of atherosclerotic plaques compared with no injection of contrast agents, which appeared black due to a lack of ultrasound contrast agents.

Moccetti et al.[204] compared differently targeted microbubbles with small peptide ligands that specifically bind to P-selectin, VCAM-1, LOX-1, and vWF in wild-type mice and double knockout mice with advanced atherosclerosis. CEUS signals were significantly higher in all four targeted microbubbles than control microbubbles, and were three to sevenfold higher in double knockout mice than in wild-type mice, with the highest signals from VCAM-1 and vWF targeted microbubbles. These results indicate that vWF and VCAM-1 targeted microbubbles hold the advantages in identifying vulnerable plaques. In addition, microbubbles can also be used to deliver genes for

atherosclerosis treatment. Petrov et al.[205] successfully designed microbubbles with lentivirus vectors for targeted gene delivery to unstable atherosclerotic plaques via active targeting using VCAM-1 antibody. The MB-mediated gene delivery could block an aneurysm formation during the progression of atherosclerosis.

Apart from the multifunctional uses of microbubbles, the exploration of nanobubbles is still limited in atherosclerosis treatment compared to in tumor treatment, opening the opportunities for the development of nanobubbles for molecular imaging and drug delivery. Wang et al.[206] developed dual targeted lipid nanobubbles for molecular imaging of vulnerable atherosclerotic plaques. Anti-VEGFR-2 ligands were conjugated onto nanobubbles through a biotin-avidin linkage system. The results indicated that the targeted nanobubbles had a uniformly nano-sized distribution with an estimated hydrodynamic diameter of about 540 nm. In-vivo CEUS imaging showed that these active- and passive-targeted lipid nanobubbles could enhance image contrast in vulnerable atherosclerotic plaques of rabbit abdominal aortas.

3.2.3. Magnetic Responsive

MNPs have multiple potential functions as molecular imaging (detection of diseases), active drug targeting, monitoring of drug intervention, hyperthermia therapy, and controlled drug release. However, MNPs in atherosclerosis management, so far, have been only focused on detection of atherosclerotic plaques and monitoring of drug intervention due to their advantages as positive- and negative-MRI contrast agents. The development of MNPs for diagnosis and therapy of atherosclerosis still needs to be further explored.

The most frequently used MRI contrast agents are gadolinium-based positive ones due to their excellence for providing brighter images (T1 image) of MRI compared with iron oxide-based negative contrast agents (IONs). However, due to the increased nephrotoxicity, the applications of all gadolinium-based contrast agents should be cautious in acute renal failure (ARF) patients.[207-209] Conversely, IONs have superior biocompatibility and safety profiles as iron is a vital element in the

human body. To avoid the disadvantages of dark MRI images, much effort has been taken to shift IONs from a negative contrast agent (T2 accelerator) to a positive contrast agent (T1 accelerator). Most IONs in pharmaceutics are based on maghemite and/or magnetite (γ-Fe2O3 and Fe3O4), which are frequently used for magnetic hyperthermia.[210] Both oxides are ferri- or ferromagnetic, respectively, with comparative crystalline structures.[211] The particle sizes of IONs determine their applications. A single ION with the size less than 20 nm is usually used for MRI in the single domain and superparamagnetic regions, whereas an ION with the particle size larger than 30 nm is usually intended for hyperthermia therapy in the single domain and multi-domain regions. However, MRI community generally divide IONs into different classes, namely very small superparamagnetic IONs (VSPIONs) with the size below 10 nm, ultrasmall superparamagnetic IONs (USPIONs) with the size between 10 and 50 nm, and superparamagnetic IONs (SPIONs) with the size between 50 and 180 nm.[212]

Recently, Nasr et al.[213] designed HA-conjugated iron oxide nanoworms (HA-NWs) for advanced atherosclerosis imaging (**Figure 10**A). The average hydrodynamic diameter of HA-NW core was around 65 ± 15 nm, corresponding to 10-20 NPs (6-nm-spherical HA-VSPIONs) forming a single chain for each NW (Figure 10B-D). The HA-NWs exhibited excellent non-invasive MRI of atherosclerotic plaques in ApoE$^{-/-}$ mice. In addition to MRI contrast agents, IONs can be also used to assess the effects of drug interventions. Two research groups[214,215] have reported the use of USPIONs to evaluate the effects of atorvastatin on plaque stability of vulnerable atherosclerotic rabbits. The results showed that atorvastatin could prevent plaque instability by suppressing the synthesis of total cholesterol (TC) in hepatocytes, upregulating the density and activity of LDL-C receptors on the surface of hepatocytes,[212] and downregulating VCAM-1 expressions[216] and MMP-9 concentrations.[217]

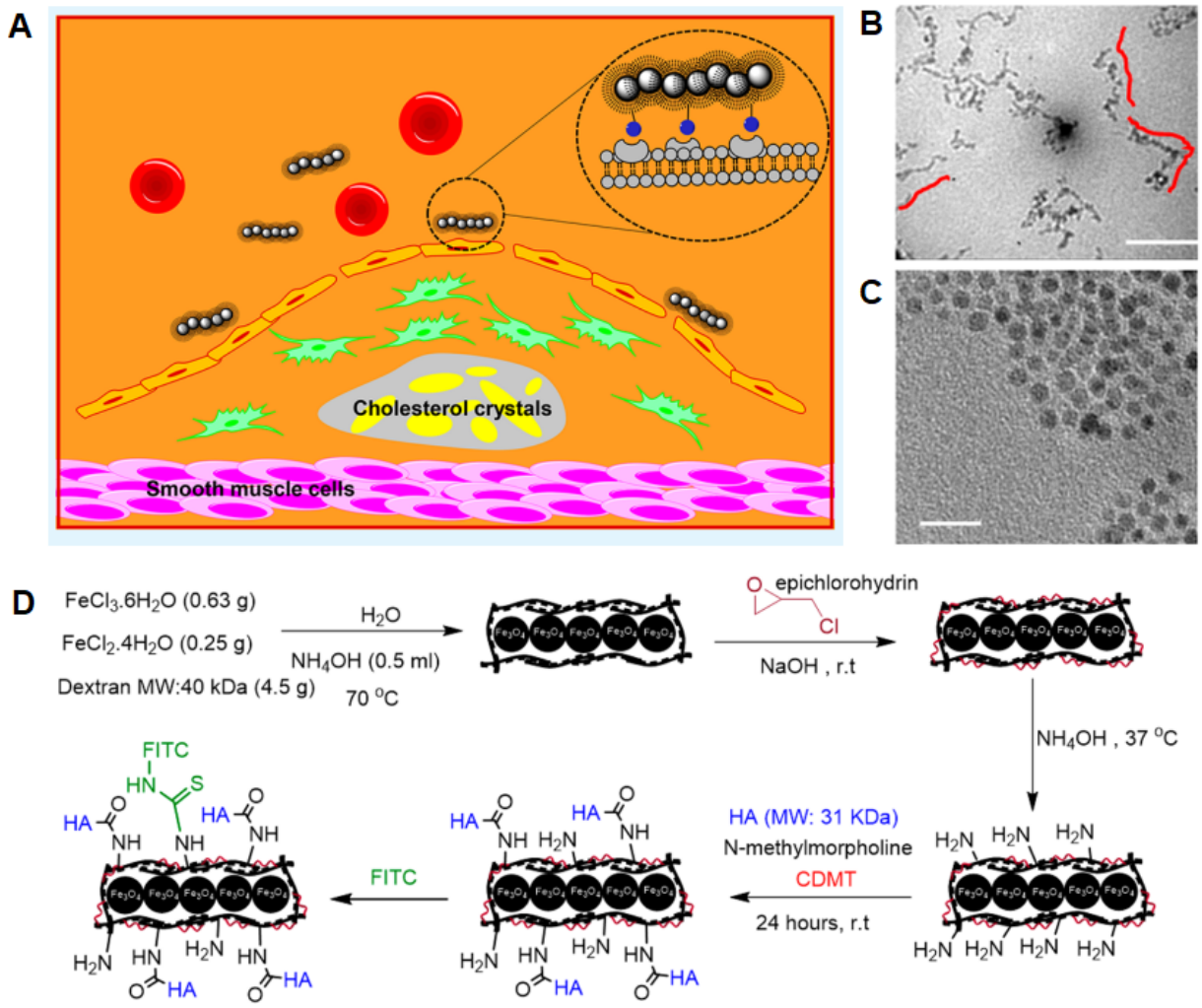

Figure 10. A) Schematic diagram of the interaction between HA-NWs and CD44 receptors. B) TEM images for HA-NWs showing their elongated shape. Three representative chains were traced with red lines. C) TEM image for HA-SPIONs showed spherical morphology. Scale bars are 50 and 20 nm for B and C, respectively. D) Synthesis of HA-NWs. Adapted with permission.[213] Copyright 2018, American Chemical Society.

An attractive combination of MNPs as contrast-enhanced MRI agents and therapy has been successfully demonstrated by Dong et al.[218] who developed USPIO-polymer-lipid hybrid nanoagents encapsulating paclitaxel (UP-NP-C11). USPIONs are effective for the detection of atherosclerotic plaques, while paclitaxel is effective for atherosclerosis treatment. The hydrophobic core of polymer-lipid hybrid nanoparticles guaranteed high loading efficiency of the hydrophobic USPIONs and paclitaxel, and the hydrophilic coating secured the superior stability and long circulation of UP-NP-C11s. The UP-NP-C11s were significantly accumulated at the atherosclerotic lesions due to the strong binding between C11s and collagen IVs, followed by internalization by macrophages and intracellular drug release. The plaques in atherosclerotic rabbits vanished after

treatment and no plaque rupture was detected, suggesting that MNPs have the potential in theranostic nanomedicine.

Another interesting idea came from Chandramouli et al.[219] who modeled SPIONs for plaque abrasion via magnetic hyperthermia. SPIONs can be targeted actively using an external alternating-current magnetic field direction to the lesion site allowing the MNPs to spin forward and backward at high velocity and finally generate heat, which lowers the plaque hardness due to transient thermal expansion. The increased temperature in magnetic hyperthermia is primarily affected by the hysteresis losses (Brownian and Neels losses), which are zero in SPIONs. The Neels restoration happens when the magnetic moment in the MNPs was reoriented.[220] In fact, the Brownian motion determines the random rotation of MNPs in the bloodstream,[221] which promotes losses after the application of a magnetic field, known as the Brownian loss. This phenomenon finally converts the energy losses to heat, which can be maximized through the appropriate choice of frequency (*f*) and strength (*H*) of the applied alternating-current magnetic field. However, to guarantee the safety of this treatment, the product *H-f* should be less than 13.4×10^8 A m^{-1} s^{-1} and the heating must be stopped after the temperature reaches 45 °C. The elevated temperature will reduce the blood viscosity leading to the reduction in drag force of MNPs. As a result, the velocity of MNPs can be easily escalated. Since the plaque volume rises in response to heat expansion, the density and tensile strength (TS) of the plaque is reduced. The velocity of SPIONs then can be controlled by the external alternating-current magnetic field. These SPIONs are used to destroy the plaque by either rotation or interchange of MNPs until the plaque disappears from the blood vessel wall through abrasion.[219]

In cancer treatment, Hayashi et al.[222] used a high-frequency magnetic field of 230 kHz and 100 Oe as the driving force for drug-release from cyclodextrins. It is noteworthy that cyclodextrins are established by seven D-glucopyranose residues linked by *R*-1,4 glycosidic bonds, which are hydrophobic inside and hydrophilic outside, thereby facilitating the encapsulation of various hydrophobic drugs. However, drugs are not chemically bound into the cyclodextrins due to the hydrophobic interaction. Drugs can be released by suppressing the hydrophobic interaction and

increasing diffusion as a result of the increased temperature achieved by magnetic hyperthermia. Furthermore, managing the temperature within 42-45 °C using the high-frequency magnetic field can enhance the effects of drugs and allow hyperthermia treatment at the same time. However, the applications of magnetic hyperthermia have yet to be fully studied for controlled release of drugs in atherosclerosis management.

3.3. Multi-Stimuli-Responsive Nanoagents

A number of works have been aiming at designing multi-stimuli-responsive nanoplatforms, as the reactivity to more than one stimulus can enhance the performance of nanoagents, such as better drug delivery efficiency to targeted sites.[78,223] In response to the multi-sensitive properties of nanoagents, Karimi et al.[224] devised the principle of nanoagent activation based on different logic gates, namely AND, OR, and their derivatives (NAND, NOR, XOR, and XNOR). The AND and OR concepts are usually chosen as the core design of multi-SRNAGs for atherosclerosis management, in which AND is the activation of SRNAGs due to the presence of several stimuli, whereas OR determines the activation by a single stimulus.

Fluorescent agents for visible fluorescence imaging (e.g., pyrene, Cy2, Cy3, Cy5, and Cy5.5 dyes)[225,226] and NIR fluorescence imaging (e.g., Cy7 dye, ICG, methylene blue, QDs, and gold nanoclusters)[226-228] are commonly combined with other stimuli-sensitive materials, owing to their advantages of cost-effectiveness, sensitivity, innate biological safety, and relative simplicity of use.[229-231] Therefore, these light-responsive agents are more popular than other responsive materials for the fabrication of multi-SRNAGs. However, other stimuli-responsive based molecular imaging agents such as MNPS and ultrasound contrast agents also have potential in combining with pH-, shear stress-, and ROS-responsive nanosystems.

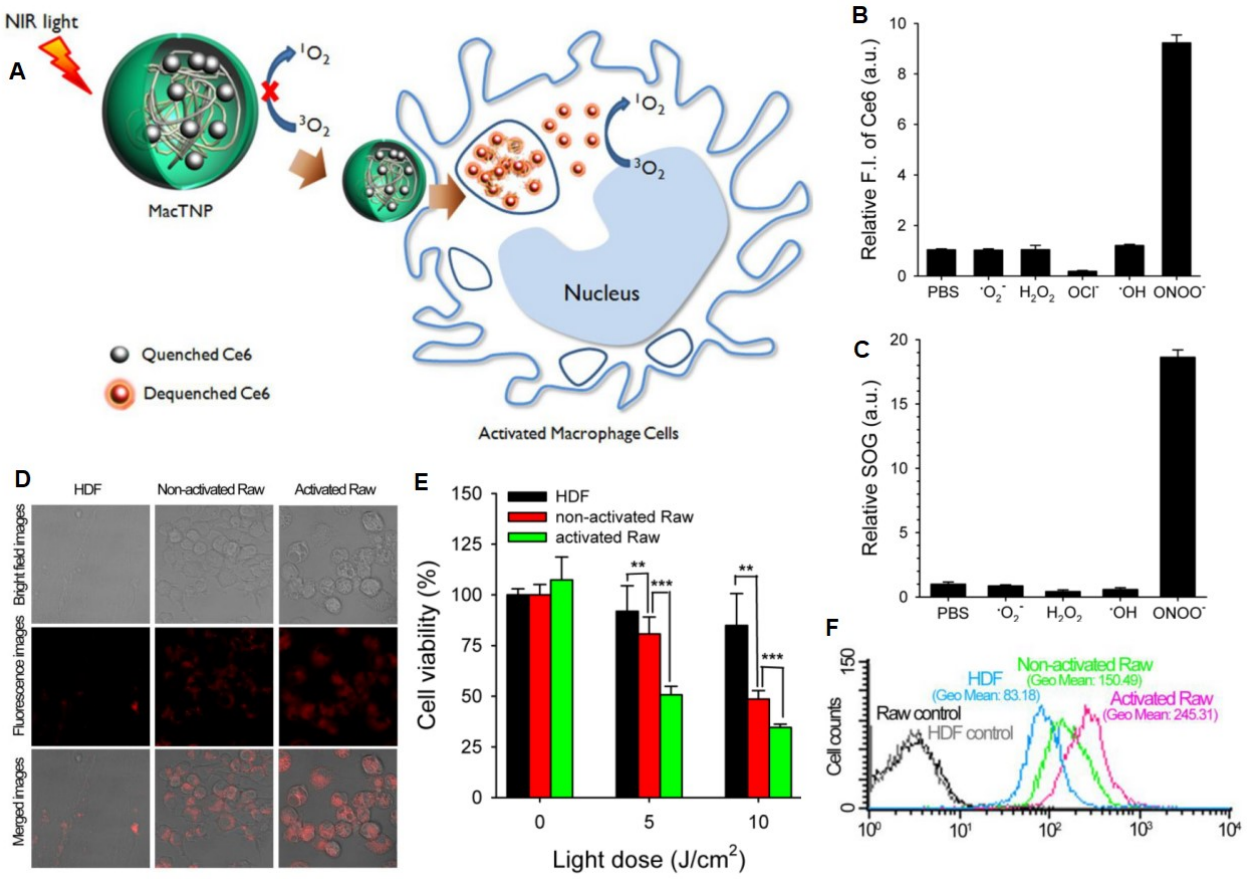

Figure 11. A) A schematic illustration of activatable nano-photomedicine for macrophage-targeted fluorescence imaging and subsequent PDT. Fluorescence and singlet oxygen generation of MacTNP are quenched in the native state. When ROS inside the activated macrophage cells degrade MacTNP, the photosensitizers (Ce6s) are de-quenched and become highly fluorescent and phototoxic. B,C) ROS-responsive recovery of fluorescence and SOG. MacTNPs were reacted with various ROS. Then, B) the Ce6 fluorescence in the samples was measured and compared with that of the control (i.e., PBS-treated MacTNP). C) Relative SOG after treatment with ROS. ROS-treated samples were irradiated using a 670-nm CW laser for 120 s, and the relative SOG was calculated by comparing the normalized SOSG fluorescence of the samples with that of the control. D) Confocal scanning fluorescence images of the MacTNP-treated HDF, non-activated and activated macrophages. E) In vitro phototoxicity test with MacTNP irradiated using a 670-nm CW laser at various light doses. F) Flow cytometric analysis of Ce6 fluorescence in HDF, non-activated and activated Raw 264.7 cells. Adapted under the terms of the CC BY-NC 4.0 license.[120] Copyright 2014, Ivyspring International Publisher.

To date, multi-stimuli-responsive AND-based nanosystems have shown great promise in enhancing drug delivery efficiency to atherosclerotic lesions. Shon et al.,[154] for instance, have developed dual-responsive theranostic nanoagents (L-SR15 agents) that were active in response to light and enzyme (cathepsin B) stimuli. Without the presence of cathepsin Bs, the L-SR15 nanoagents were still inactive. This synergistic interaction between light and enzymes built SDDSs for atherosclerosis management. The L-SR15 nanoagents were not only useful for NIRF imaging, but also could selectively deplete macrophages via PDT leading to the reduction of cathepsin B

activity.[154] Similarly, Kim et al.[120] developed dual-responsive theranostic nanoparticles (MacTNPs) that were active in response to light and ROS stimuli (**Figure 11**A). MacTNPs were still inactive (nonfluorescent and nonphototoxic) only with laser irradiation. However, when they were internalized by macrophages, the exposure to ROS, especially peroxynitrites, caused degradation of the HA coating, which resulted in the release of photosensitizers (Figure 11B). As a consequence, they emitted NIR fluorescence and generated singlet oxygen (Figure 11C) that induced macrophage apoptosis (Figure 11D-F).

Conversely, multi-stimuli-responsive OR-based nanosystems have successfully been developed by Gupta et al.[169] for pDNA delivery to VSMCs in atherosclerosis lesions. The nanocarriers were made of a pH-responsive (PPDDBP) polymer consisting of a P(DMAEMA-*co*-BMA-*co*-PAA) core-stabilizing block and PEG coating to efficiently entrap pDNAs. These nanoagents were programmed to firstly interact with ROS in the interstitial fluid, which mediated dePEGylation of polyplexes and then initiated cellular uptake of VSMCs through the interaction of positively charged PDMAEMA with the negatively charged plasma membrane of VSMCs. Finally, endosomal pH conditions promoted the destabilization of the second layer of nanocarriers and membrane disorganization leading to endosomal escape and increased pDNA transfection efficiency (**Figure 12**). Another multi-stimuli-sensitive OR-based nanosystem was shown by Ronald et al.[232] who developed myeloperoxidase sensor bis-5HTDTPA(Gd) [MPO(Gd)] for T1 (positive) MRI. These intelligent nanoagents have dual sensitivities. Firstly, MPO(Gd) is paramagnetic, so it is an effective contrast agent for MRI. Secondly, MPO(Gd) is sensitive to myeloperoxidase enzymes that is beneficial for detection of vulnerable plaques. However, due to the increased possibility of nephrotoxicity of gadolinium-based contrast agents,[207-209] ION-based positive contrast agents have become a research hotspot today.[233-236]

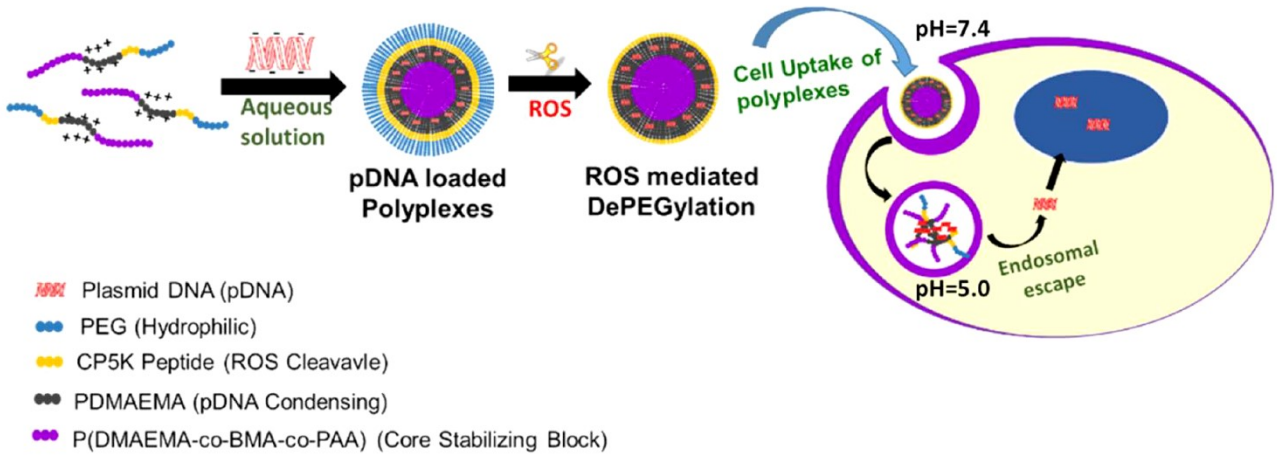

Figure 12. Illustration of extracellular ROS mediated dePEGylation of polyplexes and delivery of pDNA triggered by endosomal pH (5.0). Reproduced with permission.[169] Copyright 2015, the Royal Society of Chemistry.

Recently, Peters et al.[237] developed therapeutic nanofibers based on peptide amphiphiles (ApoA1-Ac226 PAs) that were responsive towards MMP2/9 enzymes or elevated ROS within the atherosclerotic plaques (**Figure 13**A,B). The apolipoprotein A1 (ApoA1)-mimetic peptide (Figure 13C) could enhance the active targeting to lesion sites and the Ac2-26, a peptide derived from the glucocorticoid annexin A1 protein, was released after cleavage of the peptide linkages by MMP2/9 enzymes or ROS (Figure 13D,E). These niche-responsive nanofibers, with 10% molar ratios, had median lengths of 159-174 nm and negative surface charges of around -13.9 ± 0.6 to -18.1 ± 0.5 mV, which could improve the stealthiness of nanocarriers and prolonged blood circulation. An in-vitro study showed that the therapeutic Ac2-26 could suppress pro-inflammatory macrophage activation due to its pleiotropic interactions with formyl peptide receptor 2 (FPR2) on macrophages.

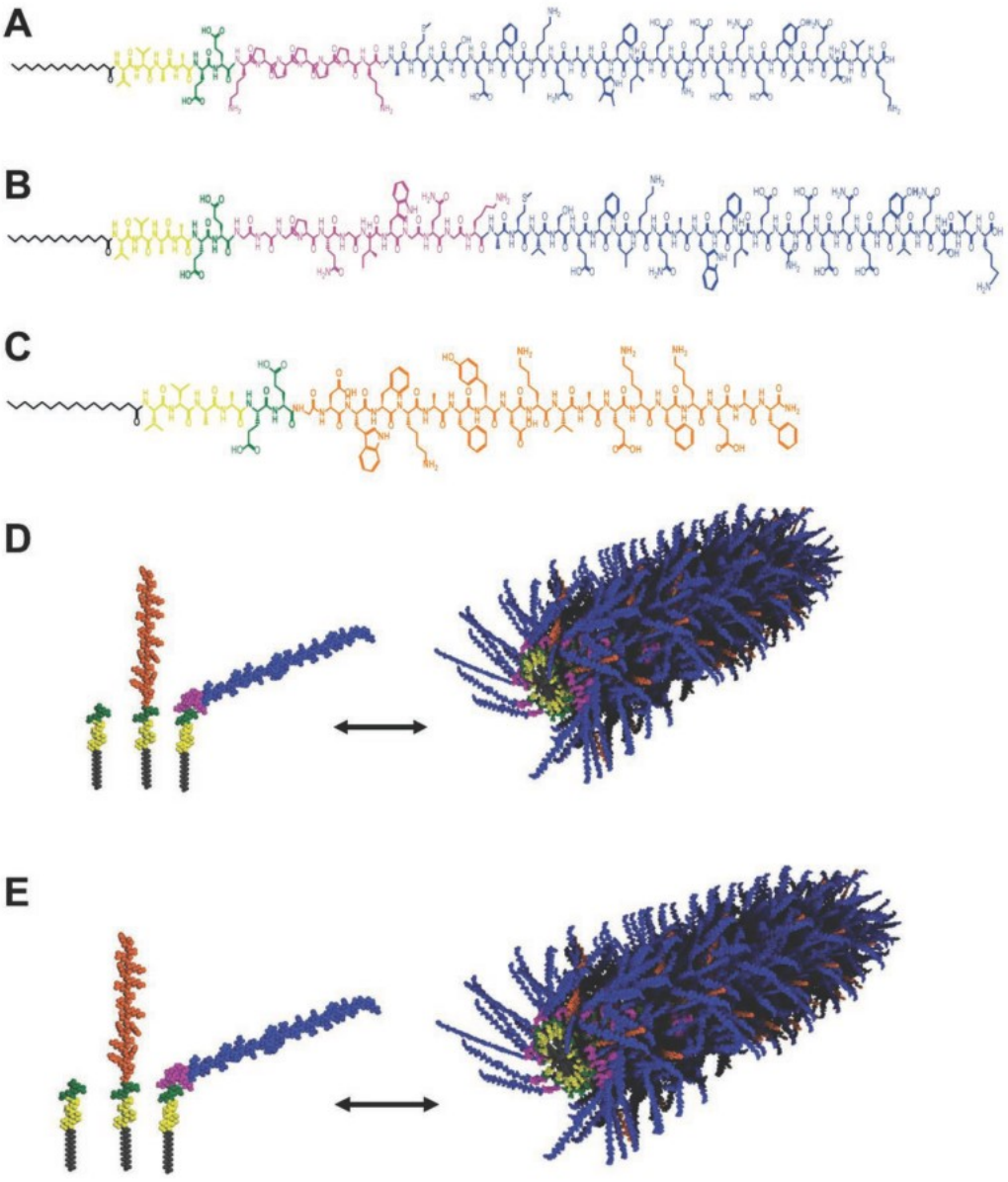

Figure 13. Chemical structures of A) ROS-Ac2-26 PA, B) MMP-Ac2-26 PA, and C) ApoA1 PA. Molecular graphics of D) ROS-Ac2-26-ApoA1 PA or E) MMP-Ac2-26-ApoA1 PA nanofibers formed by self-assembly of three PAs: the PA backbone (E2 filler PA) containing an alkyl tail (gray), β-sheet forming peptide sequence (yellow), and charged region to enhance solubility (green); ApoA1 PA with 4F peptide (orange), and PAs with pro-resolving Ac2-26 (blue) attached with a ROS- or MMP2/9-cleavable linkage (pink). Reproduced with permission.[237] Copyright 2019, WILEY-VCH.

Hong et al.[238] explored the potential of alginate-based cisplatin-loaded nanogels (TANgel) as a pH- and light-responsive nanoagent for the treatment of proliferating macrophages in atherosclerosis. This TANgel could release 100% of loaded cisplatin under acidic lysosomal pH in macrophages within 48 h, while less than 15% was released at pH 7.4. The loading efficiency of cisplatin in the nanogels was ≈13.78 ± 0.32%. The combination of NIR laser-mediated PDT of the ATTO655 fluorophores could suppress the proliferating macrophages and provide a valuable tool for NIRF

imaging. The hydrodynamic size and zeta potential of TANgel were approximately 100 nm and -28.8 mV, respectively. This theranostic TANgel showed the potential for combined chemo/radio therapy of proliferating macrophages in atherosclerotic plaques.

To improve the penetration of micro/nanobubbles as ultrasound contrast agents and assess macrophages and VSMCs in atherosclerosis, hollow silica nanospheres (HSNs) have been proposed as a new candidate contrast agent for CEUS imaging.[239-241] Recently, Ji et al.[242] introduced ferrous acetate to construct anti-CD68 receptor-targeted Fe-doped hollow silica nanoparticles (CD68-Fe-HSNs) as a dual-modal US/MRI contrast agent for identifying macrophages in atherosclerotic plaques. The shell of Fe-HSNs was composed of nano-flakes with the average diameter of 200.3 ± 15.2 nm. The in-vitro and in-vivo studies showed that PEG/Fe-HSNs had significant enhancement in contrast, which could retain its signal for 10 min, thereby satisfying the clinical needs of CEUS imaging. Futhermore, PEG/Fe-HSNs showed a clear negative contrast image for MRI. The anti-CD68 antibody improved the targeting ability of CD68-Fe-HSNs to image macrophages in atherosclerotic plaques in vivo using CEUS and MRI modalities.

4. Clinical Status of Stimuli-Responsive Nanoagents

A search on the clinicaltrial.gov website in August 2018 revealed that a total of 1,455 trials have been linked to atherosclerotic-related diseases, but only 765 trials have been completed to date. Among all of these studies, there were six clinical trials using SRNAGs for treatment and diagnosis of atherosclerosis (**Table 2**). Firstly, Kharlamov et al.[182] reported the result of a clinical trial of PTT for atherosclerosis (ClinicalTrials.gov identifier: NCT01270139). They used triple-stimuli-responsive silica-gold iron-bearing nanoparticles that were delivered to the atherosclerotic lesions using a magnetic navigation system and were responsive to ultrasound for improved targeting and imaging. The test patients received one year of NIR-mediated PTT therapy using these NPs. The result showed that PTT using these nanoagents could successfully reduce the total atheroma volume and plaque burden by ≈47.9 mm^3 and ≈39.4%, respectively. Secondly, a trial named Coronary

Atherosclerosis T1-weighed Characterization (CATCH) has just been registered (beyond FDA-defined phases) in 2018 and still has not recruited participants (ClinicalTrials.gov identifier: NCT03504956). This trial aimed to improve the diagnosis of coronary atherosclerosis using an MRI contrast agent, Gadavist, to enhance the MRI outputs for providing better image quality and reliability.

Unfortunately, a phase 1 trial (ClinicalTrials.gov identifier: NCT01436123) that studied PTT effects upon atherosclerosis using an AuNP core with a silica-iron oxide shell was terminated in 2015 under the political pressure of the Federal Security Service of the Russian Federation (FSB) and the Russian Society of Cardiology. Next in order, a study named BRIGHT-CEA (ClinicalTrials.gov identifier: NCT01873716) completed phase 1. This trial aimed to study the uptake of ICG in human carotid artery plaques for NIRF imaging.[243] ICG is an FDA-approved organic fluorescent dye[186] that has been widely used as a fluorescent imaging agent. However, ICG also possesses dual abilities as a photothermal agent for PTT[186,188] and a photosensitizer for PDT.[188,189]

Currently, a multi-purpose study has just entered phase 1 of clinical trials (ClinicalTrials.gov identifier: NCT03335020) and now it is actively recruiting participants. One of the aims of this trial is to study CEUS imaging in visualizing the arterial wall among people with atherosclerosis using an ultrasound contrast agent (Lumason, Bracco Diagnostics Inc.). Lastly, a trial named SMART-C has just entered the phase 2 of clinical trials and has not recruited participants (ClinicalTrials.gov identifier: NCT03382249). The aim of this trial was to assess the safety and efficacy of sonodynamic therapy (SDT) for atherosclerosis management. SDT is categorized as a novel treatment for carotid atherosclerotic plaques. This trial will use sinoporphyrin sodium (DVDMS), a new sonosensitizer agent, to generate ROS, especially singlet oxygen, by an ultrasound trigger. This SDT-mediated singlet oxygen generation can deplete macrophages and inhibit the degradation of ECM leading to plaque stabilization and reduction. Furthermore, SDT has recently been studied for cancer therapy.[244-246] This is a new promising treatment that still needs to be further explored for atherosclerosis management.

5. Conclusions and Perspectives

We have entered the era of nanotechnology that enables us to combat diseases at the molecular level by engineering smart nanoagents with versatile functionality. Significant advances in nanoengineering enable the combination of organic and inorganic nanomaterials into hybrid nanoagents that can be programmed to autonomously navigate in the bloodstream, overcome biological barriers, and assemble with their nano-cohort at the targeted lesion. The assembly of nanoagents with endogenous and exogenous stimuli breaks down their shells, facilitates intracellular delivery, releases their cargo to kill the corrupt cells, and enhances imaging capability. All of these improvements show great potential to apply personalized medicine in atherosclerosis management. To achieve this potential, we need SDDSs that are reactive to endogenous (ROS, enzymes, pH, and shear stress) and/or exogenous (light, ultrasound, and magnetic field) triggers. By integrating the nanoagents and drugs into diverse stimuli-responsive systems, it can fine-tune the SRNAGs and release the drugs to the specifically targeted sites for the treatment of corrupt cells.

Firstly, we should understand the biological environment around atherosclerotic lesions as it can help us to precisely design nanoagents that are specifically active upon one stimulus or several stimuli from the surroundings. In atherosclerotic lesions, the overproduction of ROS promotes Ox-LDL accumulation, endothelial dysfunction, DNA damage, leukocyte migration and differentiation, VSMC proliferation, and collagen degradation by MMPs.[68] This excessive ROS generation can be a specific trigger for drug release and activation of SRNAGs. SOD-mimetic nanoparticles or nanozymes have recently been explored for their potential in nanomedicine,[93] such as CeO_2 that can suppress excessive ROS production in atherosclerosis.[100]

In addition, many enzymes are present in atherosclerotic plaques, such as MMPs, hyaluronidases, and cathepsins and play a central role in the degradation of ECM. However, it is important to design nanoagents that are reactive towards these pro-atherosclerotic enzymes and have efficacy to inhibit and reduce their activities. Furthermore, extracellular fluid pH in inflammatory sites has been known for a number of years to be acidic.[159] The hypoxic condition of atherosclerotic lesions promotes

protruding lactate concentrations due to the deposition of activated macrophages that actively engulf Ox-LDL and require an extremely high energy demand that force macrophages to use anaerobic glycolysis for ATP production.[160,161] The slightly acidic interstitial fluids (pH around 6.0 to 6.8) in atherosclerotic lesions[163] and the acidic lysosomal conditions (pH below 5) in macrophages[164] can be used to control drug release. Last but not least, the narrowing blood vessels promote elevated hemodynamic WSS in the constricted sites up to 70-100 dyn cm^{-2} or even higher.[5] This abnormal WSS can be used as a stimulus to trigger cargo release and local delivery of drugs and imaging agents to the sites of vulnerable plaques.

Nowadays, contrast agents are gaining popularity as molecular imaging enhancers of prominent imaging modalities such as MRI,[86] CEUS imaging,[87] NIRF imaging,[88] and PAI,[89] which can improve image resolution and enable real-time imaging. Therefore, it is paramount to design SRNAGs that can be detected by the imaging modalities via light-, ultrasound-, or magnetic field-activation. Interestingly, as well as their molecular imaging uses, some inorganic nanoparticles such as AuNPs,[91] IONs,[92] and copper sulfide nanoparticles[93] possess additional theranostic capability all in a single nanoparticle. Furthermore, the multi-potential uses of inorganic nanoparticles can be optimized by combination with organic nanoparticles to prolong the circulation of nanoagents in the blood and improve drug delivery efficiency and imaging functionality.

Fluorescent agents for visible fluorescence imaging and NIR fluorescence imaging are commonly combined with other stimuli-sensitive materials, owing to their advantages of cost-effectiveness, sensitivity, innate biological safety, and relative simplicity of use.[229-231] For instance, the Cy5 dye has been widely used as a fluorescent imaging agent in ROS-, enzyme-, and pH-responsive nanoplatforms.[114,117,128,147,152,165,169] Meanwhile, ICG is an example of NIR fluorescent imaging agents that not only can be used for imaging, but also for PTT[187,188] and PDT.[188,189] More importantly, ICG could also be used for light-triggered drug release when loaded into liposomes.[191]

In addition, ultrasound contrast agents still need to be further developed for theranostic purposes as they have great potential in the near future as low-cost theranostic nanoagents. The dimension of

microbubbles also needs to be reduced to nanoscale sizes for enabling both the EPR effect and increased nanoparticle uptake via active targeting. On top of that, microbubbles and nanobubbles can be triggered using high acoustic power ultrasound for controlled drug release that enables local delivery of drugs via sonoporation.[196,197] Hollow silica nanospheres (HSNs) have currently been proposed as a new candidate contrast agent for CEUS imaging.[239-241] Additionally, the potential of SDT for atherosclerosis management is promising and has entered phase 2 of clinical trials (ClinicalTrials.gov identifier: NCT03382249). The use of a sonosensitizer agent, such as DVDMS, can generate ROS, especially singlet oxygen, by an ultrasound trigger. This SDT-mediated singlet oxygen generation can deplete macrophages and inhibit the degradation of ECM leading to plaque stabilization and reduction. Also, MNPs can be further explored not only for molecular imaging and active drug targeting but also for hyperthermia therapy and controlled drug release. However, IONs should be shifted from T2 to T1 accelerators to improve the image quality.

The exploration of stimuli-sensitive micro and/or nanomaterials with good biocompatibility and excellent properties is predicted to increase in the near future. Nanogels can be one of the excellent candidates for SRNAGs. Nanogels or hydrogel nanoparticles have the ability to encapsulate different biologically active molecules such as drugs, proteins, and genes and can be programmed to release the cargo via different external stimuli, such as light, ultrasound, electric field, and magnetic field or internal stimuli, such as pH, temperature, enzymes, and redox potential.[247-250]

Interestingly, “back to nature” is one of the most effective strategies to improve the biocompatibility and safety of nano-drug formulation. Currently, the bacterial mechanosensitive channel of large conductance (MscL) has withdrawn much attention as a triggered nanovalve for drug release. In bacteria, the MscL functions to protect cells from lysis upon severe hypoosmotic shock.[250] The MscL has an extremely large pore when opening, ≈3 nm in diameter, and can be purified and reconstituted into artificial membranes.[252] A number of studies have been conducted to explore the potential of reconstituted MscL nanovalves as gates for controlled drug release using various stimuli such as ultraviolet (UV) light,[253] acidic pH,[254,255] and magnetic field.[256,257] These smart MscL-

based nanoagents will soon dominate the exploration of SRNAGs for cardiovascular diseases and cancer. In conclusion, SRNAGs have shown excellent progress in preclinical studies over the past ten years and need to be encouraged to enter the clinical trials.

Table 1. Recent Advances in Stimuli-Responsive Theranostic Nanoagents for Atherosclerosis.

Stimulus	Nanocarrier	Nanoagent (abbreviation)	Imaging	Therapy	Target	Ref.
Reactive oxygen species (ROS)	*β*-cyclodextrin (*β*-CDs)	Broad-spectrum reactive oxygen species scavenging nanoparticles (TPCD NPs)	Fluorescence imaging	Nanozymes (ROS scavenging)	Macrophages and VSMCs (in vitro and in vivo)	[111]
	Hybrid poly(ethylene glycol)-cerium oxide (hibrid PEG-CeO_2)	H_2O_2-responsive and plaque-penetrating nanoplatform (S2P-CeO_2-ASO)	Fluorescence imaging	siRNA	Macrophage-derived foam cells (in vitro and in vivo)	[114]
	β-cyclodextrin (*β*-CDs)	ROS-sensitive *β*-cyclodextrin nanoparticles (Ox-bCD NPs)	Fluorescence imaging	Rapamycin (RAP)	Macrophage-derived foam cells (in vitro and in vivo)	[117]
Enzymes	*N,N'*-bis(benzyl)pyrimidine-4,6-dicarboxamide	Radiolabeled inhibitors (MMP-13 inhibitors)	PET	Inbibition of MMP-13s	MMP-13 enzymes (in vitro and in vivo)	[127]
	Iron oxide	ION-based MMP-13 inhibitors (MMP13i-A agents)	Fluorescence imaging	MMP13i-A	MMP-13 enzymes (in vitro and in vivo)	[128]
	N-benzenesulfonyliminodiacetyl monohydroxamates and *N*-halophenoxy-benzenesulfonyl iminodiacetyl monohydroxamates	MMP2/9 inhibitors (no abbreviation)	SPECT	MMP2/9 inhibitors with Iodine-123 (^{123}I)	MMP-2 and MMP-9 enzymes (in vitro and in vivo)	[138]
	(*R*)-2-(4-(4-fluorobenzamido)phenylsulfonamido)-3-(1H-indol-3-yl)propanoic acid and methyl 4-[3-(formylhydroxyamino)-4-(4-(4-trifluoromethoxyphenoxy)phenylsulfonyl)butyl]benzoate	MMP-2/MMP-9 inhibitor ^{18}F-1 and MMP-9 inhibitor ^{3}H-2 (no abbreviation)	PET	MMP-2/MMP-9 inhibitor ^{18}F-1 and MMP-9 inhibitor ^{3}H-2	MMP-2 and MMP-9 enzymes (in vitro and in vivo)	[140]
	Reconstituted high density lipoprotein (r-HDL)	Lovastatin loaded-hyaluronic acid-decorated reconstituted high-density lipoprotein (HA-LT-r-HDL) and Simvastatin-loaded hyaluronic acid-decorated PLGA-reconstituted high-density lipoprotein (ST-HA-(C)-PLGA-r-HDL)	Fluorescence and NIRF imaging	Lovastatin and simvastatin	Macrophage-derived foam cells (in vitro and in vivo)	[147,148]

Table 1. Recent Advances in Stimuli-Responsive Theranostic Nanoagents for Atherosclerosis (cont.).

Stimulus	Nanocarrier	Nanoagent (abbreviation)	Imaging	Therapy	Target	Ref.
Enzymes	Nanocomplexes	Hyaluronic-acid-coated LOX-1-specific siRNA-condensed cell-penetrating peptide nanocomplexes (HA-coated CPPs/siRNA NPs)	Fluorescence imaging	siRNA	Macrophage-derived foam cells (in vitro and in vivo)	[152]
pH	Poly(ethylene glycol) (PEG)	Tannic acid-iron complexes (TA NPs)	Fluorescence imaging	Antioxidant (tannic acid)	Activated macrophages (in vitro)	[165]
	Hyaluronic acid-polypyrrole nanoparticles (HA-PPyNPs)	Doxorubicin-loaded hyaluronic acid-polypyrrole nanoparticles (DOX@HA-PPyNPs)	Fluorescence imaging	Doxorubicin (DOX)	Activated macrophages (in vitro)	[168]
	β-cyclodextrin (β-CDs)	Acetalated β-cyclodextrin nanoparticles (Ac-bCD NPs)	Fluorescence imaging	Rapamycin (RAP)	Macrophage-derived foam cells (in vitro and in vivo)	[117]
Shear stress	Amide-bearing 1,3-dipalmitamido propan-2-yl 2-(trimethylammonio)ethyl phosphate (Pad-PC-Pad)	Amide-bearing 1,3-dipalmitamidopropan-2-yl 2-(trimethylammonio)ethyl phosphate lenticular vesicles (Pad-PC-Pad LUVET$_{100}$)	Fluorescence imaging	Carboxyfluo-rescein (a model drug)	Local delivery of drugs to the atherosclerotic plaques (in vitro)	[176]
Light	Silica and microbubbles	Silica-gold iron-bearing nanoparticles with targeted microbubbles (no abbreviation)	Quantitative coronary angiography (QCA) and intravascular ultrasound (IVUS)	PTT	Atherosclerotic lesions in human (First-in-man Trial)	[181]
	Copper sulfide (CuS) nanoparticles	TRPV1 antibody-coupled copper sulfide nanoparticles (CuS-TRPV1)	Ultrasound and PAI	PTT	VSMCs (in vitro and in vivo)	[182]
	Silica nanoparticles	Mesoporous silica-coated upconversion fluorescent NPs encapsulating chlorin e6 (UCNPs-Ce6)	NIR-visible imaging	PDT	Macrophage-derived foam cells (in vitro)	[183]
	Dextran sulfate-deoxycholic acid (DS-DOCA) nanoparticles	Dextran sulfate-deoxycholic acid nanoparticles encapsulating chlorin e6 (Ce6/DS-DOCA NPs)	Fluorescence imaging	PDT	Activated macrophages (in vitro)	[185]
	Human serum albumin (HSA)	Human serum albumin (HSA)-based theranostic nanoagents encapsulating ICG and sirtuin 1 (Sirt1) activator SRT1720 (ICG/SRT@HSA-pept NMs)	NIRF imaging	Sirtuin 1 (Sirt1) activator SRT172	VSMCs (in vitro and in vivo)	[190]

Table 1. Recent Advances in Stimuli-Responsive Theranostic Nanoagents for Atherosclerosis (cont.).

Stimulus	Nanocarrier	Nanoagent (abbreviation)	Imaging	Therapy	Target	Ref.
Light	Liposomes	Indocyanine green-loaded liposomes (ICG-liposomes)	NIRF imaging	Calcein and FITC-Dextran 20 kDa (small and large molecule-model drugs)	Non-cancer cells (e.g. macrophages in atherosclerosis)	[191]
Ultrasound	Polymeric microbubbles	Simvastatin-loaded polymeric microbubbles (S-MBs)	CEUS imaging	Simvastatin	Local delivery of drugs to the atherosclerotic plaques (in vitro)	[203]
	Microbubbles	Not specified	CEUS imaging	Gene therapy	Inhibit an aneurysm formation due to atherosclerosis	[205]
Magnetic field	Poly(D,L-lactide-*co*-glycolide) (PLGA), 1,2-distearoyl-*sn*-glycero-3-phosphoethanolamine-*N*-[maleimide(polyethylene glycol)-2000] (ammonium salt) (DSPE-PEG-Mal), and soybean lecithin	USPIO-polymer-lipid hybrid nanoagents encapsulating paclitaxel (UP-NP-C11)	MRI	Paclitaxel	Activated macrophages (in vitro and in vivo)	[218]
	Superparamagnetic iron oxide nanoparticles (SPIONs)	Superparamagnetic iron oxide nanoparticles (SPIONs)	MRI	Plaque abrasion via magnetic hyperthermia	Atherosclerotic plaques (a theoretical study)	[219]
Light and ROS	Hybrid Ce6-HA	ROS-responsive theranostic nanoparticles (MacTNPs)	NIRF imaging	PDT	Activated macrophages (in vitro)	[121]
Light and enzymes	Hybrid Ce6-conjugated PEG graft-poly(L-lysine)	Protease-mediated theranostic agents (L-SR15 agents)	NIRF imaging	PDT	Activated macrophages (in vitro and in vivo)	[154]
pH and ROS	P(DMAEMA-*co*-BMA-*co*-PAA) core-stabilizing block and PEG (PPDDBP)	PPDDBP/pDNA polyplexes	Fluorescence imaging	pDNA	VSMCs (in vitro)	[169]
Enzymes and ROS	Peptide amphiphiles (PAs)	Therapeutic nanofibers based on peptide amphiphiles (ApoA1-Ac226 PAs)	Fluorescence imaging	Therapeutic Ac2-26 peptides	Activated macrophages (in vitro)	[237]
pH and light	Nanogels	Alginate-based cisplatin-loaded nanogels (TANgel)	NIRF imaging	Cisplatin	Proliferating macrophages (in vitro)	[238]

Table 2. Stimuli-Responsive Nanoagents for Atherosclerosis in Clinical Trials.

Stimulus	Nanocarrier	Nanoagent (abbreviation)	Intervention/ treatment	Recruitment status	Clinical status	Ref.
Light, ultrasound, and magnetic field	Silica and microbubbles	Silica-gold iron-bearing nanoparticles with targeted microbubbles (no abbreviation)	PTT	Completed	Not applicable	NCT01270139 [181]
Magnetic field	Gadolinium-based contrast agents	Gadavist (Gadavist)	Metoprolol	Not yet recruiting	Not applicable	NCT03504956
Light	Iron oxide-silica	AuNPs with iron oxide-silica shells (no abbreviation)	PTT	Terminated (under the political pressure of the Federal Security Service of the Russian Federation (FSB) and the Russian Society of Cardiology)	Phase 1	NCT01436123
Light	Indocyanine green (ICG)	Indocyanine green (ICG)	No drug intervention	Completed	Phase 1	NCT01873716 [243]
Ultrasound	Microbubbles	Lumason (Lumason ; Bracco Diagnostics, Inc.)	No drug intervention	Recruiting	Phase 1	NCT03335020
Ultrasound	Not identified	Sinoporphyrin sodium (DVDMS)	Sonodynamic therapy (SDT)	Not yet recruiting	Phase 2	NCT03382249

Note : not applicable is used to describe trials without FDA-defined phases, including trials of devices or behavioral interventions; ClinicalTrials.gov.

Acknowledgements

Financial support from the National Natural Science Foundation of China (11572064, 51603023), Fundamental Research Funds for the National Key R&D Project (2016YFC1102305), Fundamental Research Funds for Central Universities (2018CDHB1B08, 2018CDXYSW0023, 106112016CDJXY230002, 106112018CDPTCG0001-10), and the Chongqing Research Program of Basic research and Frontier Technology (cstc2017jcyjAX0186) are gratefully acknowledged.

Conflict of Interest

The authors declare no conflict of interest.

Keywords

stimuli-responsive, nanoagents, atherosclerosis

References

[1] G. A. Roth, C. Johnson, A. Abajobir, F. Abd-Allah, S. F. Abera, G. Abyu, M. Ahmed, B. Aksut, T. Alam, K. Alam, F. Alla, N. Alvis-Guzman, S. Amrock, H. Ansari, J. Ärnlöv, H. Asayesh, T. M. Atey, L. Avila-Burgos, A. Awasthi, A. Banerjee, A. Barac, T. Bärnighausen, L. Barregard, N. Bedi, K. E. Belay, D. Bennett, G. Berhe, Z. Bhutta, S. Bitew, J. Carapetis, J. J. Carrero, D. C. Malta, C. A. Castañeda-Orjuela, J. Castillo-Rivas, F. Catalá-López, J. Y. Choi, H. Christensen, M. Cirillo, L. Jr. Cooper, M. Criqui, D. Cundiff, A. Damasceno, L. Dandona, R. Dandona, K. Davletov, S. Dharmaratne, P. Dorairaj, M. Dubey, R. Ehrenkranz, M. E. S. Zaki, E. J. A. Faraon, A. Esteghamati, T. Farid, M. Farvid, V. Feigin, E. L. Ding, G. Fowkes, T. Gebrehiwot, R. Gillum, A. Gold, P. Gona, R. Gupta, T. D. Habtewold, N. Hafezi-Nejad, T. Hailu, G. B. Hailu, G. Hankey, H. Y. Hassen, K. H. Abate, R. Havmoeller, S. I. Hay, M. Horino, P. J. Hotez, K. Jacobsen, S. James, M. Javanbakht, P. Jeemon, D. John, J. Jonas, Y. Kalkonde, C. Karimkhani, A. Kasaeian, Y. Khader, A. Khan, Y. H. Khang, S. Khera, A. T. Khoja, J. Khubchandani, D. Kim, D. Kolte, S. Kosen, K. J. Krohn, G. A. Kumar, G. F. Kwan, D. K. Lal, A. Larsson, S. Linn, A. Lopez, P. A. Lotufo, H. M. A. E. Razek, R. Malekzadeh, M. Mazidi, T. Meier, K. G. Meles, G., Mensah, A. Meretoja, H. Mezgebe, T. Miller, E. Mirrakhimov, S. Mohammed, A. E. Moran, K. I. Musa, J. Narula, B. Neal, F. Ngalesoni, G. Nguyen, C. M. Obermeyer, M. Owolabi, G. Patton, J. Pedro, D. Qato, M. Qorbani, K. Rahimi, R. K. Rai, S. Rawaf, A. Ribeiro, S. Safiri, J. A. Salomon, I Santos, M. M. Santric, B. Sartorius, A. Schutte, S. Sepanlou, M. A. Shaikh, M. J. Shin, M. Shishehbor, H. Shore, D. A. S. Silva, E. Sobngwi, S. Stranges, S. Swaminathan, R. Tabarés-Seisdedos, A. N. Tadele, F. Tesfay, J. S. Thakur, A. Thrift, R. Topor-Madry, T. Truelsen, S. Tyrovolas, K. N. Ukwaja, O. Uthman, T. Vasankari, V. Vlassov, S. E. Vollset, T. Wakayo, D. Watkins, R. Weintraub, A. Werdecker, R. Westerman, C. S. Wiysonge, C. Wolfe, A. Workicho, G. Xu, Y. Yano, P. Yip, N. Yonemoto, M. Younis, C. Yu, T. Vos, M. Naghavi, C. Murray, *J. Am. Coll. Cardiol.* **2017**, *70*, 1.

[2] World Health Organization (WHO): Cardiovascular diseases (CVDs). http://www.who.int/en/news-room/fact-sheets/detail/cardiovascular-diseases-(cvds). Accessed on 16 August 2018.

[3] B. Liu, D. Tang, *Mol. Cell. Biomech.* **2010**, *7*, 193.

[4] S. Slysh, S. Goldberg, J. P. Dervan, A. Zalewski, *Am. Heart J.* **1985**, *109*, 744.

[5] C. Cheng, F. Helderman, D. Tempel, D. Segers, B. Hierck, R. Poelmann, A. van Tol, D. J. Duncker, D. Robbers-Visser, N. T. Ursem, R. van Haperen, J. J. Wentzel, F. Gijsen, A. F. van der Steen, R. de Crom, R. Krams, *Atherosclerosis* **2007**, *195*, 225.

[6] K. Zhang, Y. Chen, T. Zhang, L. Huang, Y. Wang, T. Yin, J. Qiu, H. Gregersen, G. Wang, *Ann. Biomed. Eng.* **2018**, *46*, 849.

[7] W. Jr. Insull, *Am. J. Med.* **2009**, *122*, S3.

[8] C. Michiels, *J. Cell. Physiol.* **2003**, *196*, 430.

[9] J. W. Yau, H. Teoh, S. Verma, *BMC Cardiovasc. Disord.* **2015**, *15*, 130.

[10] K. Dharmashankar, M. E. Widlansky, *Curr. Hypertens. Rep.* **2010**, *12*, 448.

[11] A. Leone, *Curr. Pharm. Des.* **2015**, *21*, 4370.

[12] J. Han, A. K. Mandal, L. M. Hiebert, *Cardiovasc. Diabetol*. **2005**, *4*, 12.

[13] E. A. Fisher, J. E. Feig, B. Hewing, S. L. Hazen, J. D. Smith, *Arterioscler., Thromb., Vasc. Biol.* **2012**, *32*, 2813.

[14] J. Millán, X. Pintó, A. Muñoz, M. Zúñiga, J. Rubiés-Prat, L. F. Pallardo, L. Masana, A. Mangas, A. Hernández-Mijares, P. González-Santos, J. F. Ascaso, J. Pedro-Botet, *Vasc. Health Risk Manage.* **2009**, *5*, 757.
[15] X. Xie, J. Tan, D. Wei, D. Lei, T. Yin, J. Huang, X. Zhang, J. Qiu, C. Tang, G. Wang, *J. R. Soc., Interface* **2013**, *10*, 20121053.
[16] D. Wei, Y. Chen, C. Tang, H. Huang, L. Liu, Z. Wang, R. Li, G. Wang, *Ann. Biomed. Eng.* **2013**, *41*, 611.
[17] Y. Nakashima, E. W. Raines, A. S. Plump, J. L. Breslow, R. Ross, *Arterioscler., Thromb., Vasc. Biol.* **1998**, *18*, 842.
[18] A. S. Storch, J. D. de Mattos, R. Alves, I. S. Galdino, H. N. M. Rocha, *Int. J. Cardiovasc. Sci.* **2017**, *30*, 262.
[19] Y. Ohara, T. E. Peterson, D. G. Harrison, *J. Clin. Invest.* **1993**, *91*, 2546.
[20] M. K. Cathcart, *Arterioscler., Thromb., Vasc. Biol.* **2004**, *24*, 23.
[21] A. J. Kattoor, N. V. K. Pothineni, D. Palagiri, J. L. Mehta, *Curr. Atheroscler. Rep.* **2017**, *19*, 42.
[22] M. T. Quinn, S. Parthasarathy, L. G. Fong, D. Steinberg, *Proc. Natl. Acad. Sci. U. S. A.* **1987**, *84*, 2995.
[23] S. Becker, M. K. Warren, S. Haskill, *J. Immunol.* **1987**, *139*, 3703.
[24] E. Montanari, S. Stojkovic, C. Kaun, C. E. Lemberger, R. de Martin, S. Rauscher, M. Gröger, G. Maurer, C. Neumayer, I. Huk, K. Huber, S. Demyanets, J. Wojta, *J. Thromb. Haemostasis* **2016**, *116*, 317.
[25] D. A. Chistiakov, Y. V. Bobryshev, A. N. Orekhov, *J. Cell. Mol. Med.* **2016**, *20*, 17.
[26] H. B. Brewer Jr., *J. Clin. Invest.* **2000**, *105*, 703.
[27] C. C. Hedrick, *Arterioscler., Thromb., Vasc. Biol.* **2015**, *35*, 253.
[28] R. Kleemann, S. Zadelaar, T. Kooistra, *Cardiovasc. Res.* **2008**, *79*, 360.
[29] A. D. Lucas, D. R. Greaves, *Expert Rev. Mol. Med.* **2001**, *3*, 1.
[30] P. E. DiCorleto, D. F. Bowen-Pope, *Proc. Natl. Acad. Sci. U. S. A.* **1983**, *80*, 1919.
[31] E. M. Rzucidlo, K. A. Martin, R. J. Powell, *J. Vasc. Surg.* **2007**, *45*, A25.
[32] M. Ponticos, B. D. Smith, *J. Biomed. Res.* **2014,** *28*, 25.
[33] P. Yan, C. Xia, C. Duan, S. Li, Z. Mei, *Int. J. Biol. Sci.* **2011**, *7*, 937.
[34] T. Aoyama, M. Chen, H. Fujiwara, T. Masaki, T. Sawamura, *FEBS Lett.* **2000**, *467*, 217.
[35] I. Tabas, *Arterioscler., Thromb., Vasc. Biol.* **2005**, *25*, 2255.
[36] M. M. Mughal, M. K. Khan, J. K. DeMarco, A. Majid, F. Shamoun, G. S. Abela, *Expert Rev. Cardiovasc. Ther.* **2011**, *9*, 1315.
[37] M. C. Clarke, T. D. Littlewood, N. Figg, J. J. Maguire, A. P. Davenport, M. Goddard, M. R. Bennett, *Circ. Res.* **2008**, *102*, 1529.
[38] P. R. Moreno, K. R. Purushothaman, M. Sirol, A. P. Levy, V. Fuster, *Circulation* **2006**, *113*, 2245.
[39] P. R. Moreno, K. R. Purushothaman, E. Zias, J. Sanz, V. Fuster, *Curr. Mol. Med.* **2006**, *6*, 457.
[40] A. C. Newby, *Trends Cardiovasc. Med.* **2007**, *17*, 253.
[41] Y. Wang, J. Qiu, S. Luo, X. Xie, Y. Zheng, K. Zhang, Z. Ye, W. Liu, H. Gregersen, G. Wang, *Regener. Biomater.* **2016**, *3*, 257.
[42] J. Qiu, D. Lei, J. Hu, T. Yin, K. Zhang, D. Yu, G. Wang, *Regener. Biomater.* **2017**, *4*, 215.
[43] Z. Y. Li, S. Howarth, R. A. Trivedi, J. M. U-King-Im, M. J. Graves, A. Brown, L. Wang, J. H. Gillard, *J. Biomech.* **2006**, *39*, 2611.
[44] T. Thim, M. K. Hagensen, J. K. Bentzon, E. Falk, *J. Intern. Med.* **2008**, *263*, 506.
[45] M. Li, T. Yin, Y. Wang, F. Dua, X. Zou, H. Gregersen, G. Wang, *Mater. Sci. Eng., C* **2014**, *43*, 641.
[46] X. Wu, G. Wang, C. Tang, D. Zhang, Z. Li, D. Du, Z. Zhang, *J. Biomed. Mater. Res., Part A* **2011**, *98A*, 442.
[47] Q. Zhang, Y. Shen, C. Tang, X. Wu, Q. Yu, G. Wang, *J. Biomed. Mater. Res., Part B* **2015**, *103*, 464.

[48] X. Wu, T. Yin, J. Tian, C. Tang, J. Huang,Y. Zhao, X. Zhang, X. Deng, Y. Fan, D. Yu, G. Wang, *Regener. Biomater.* **2015**, *2*, 87.
[49] D. Sun, Y. Zheng, T. Yin, C. Tang, Q. Yu, G. Wang, *J. Biomed. Mater. Res., Part A* **2014**, *102*, 1625.
[50] K. Inoue, *Thrombosis* **2012**, *2012*, 1.
[51] Y. Zhao, R. Du, T. Zhou, D. Yang, Y. Huang, Y. Wang, J. Huang, X. Ma, F. He, J. Qiu, G. Wang, *Adv. Healthcare Mater.* **2018**, *7*, 1800207.
[52] R. Du, Y. Wang, Y. Huang, Y. Zhao, D. Zhang, D. Du, Y. Zhang, Z. Li, S. McGinty, G. Pontrelli, T. Yin, G. Wang, *NPG Asia Mater.* **2018**, *10*, 642.
[53] T. Hu, C. Yang, M. Fu, J. Yang, R. Du, X. Ran, T. Yin, G. Wang, *Regener. Biomater.* **2017**, *4*, 167.
[54] T. Hu, S. Lin, R. Du, M. Fu, Q. Rao, T. Yin. Y. Huang, G. Wang, *Biomater. Sci.* **2017**, *5*, 1845.
[55] T. Hu, J. Yang, K. Cui, Q. Rao, T. Yin, L. Tan, Y. Zhang, Z. Li, G. Wang, *ACS Appl. Mater. Interfaces* **2015**, *7*, 11695.
[56] J. van Werkum, T. Godschalk, T. Oirbans, J. ten Berg, *Interv. Cardiol.* **2011**, *3*, 581.
[57] A. P. Nikalje, *Med. chem.* **2015**, *5*, 081.
[58] K. Y. Choi, G. Liu, S. Lee, X. Chen, *Nanoscale* **2012**, *4*, 330.
[59] C. K. W. Chan, L. Zhang, C. K. Cheng, H. Yang, Y. Huang, X. Y. Tian, C. H. J. Choi, *Small* **2018**, *14*, 1702793.
[60] Z. Li, *Ther. Delivery* **2017,** *8*, 597.
[61] W. Wu, W. Wang, J. S. Li, *Prog. Polym. Sci.* **2015**, *46*, 55.
[62] W. Wu, C. Ye, H. Xiao, X. Sun, W. Qu, X. Li, M. Chen, J. S. Li, *Int. J. Pharm*. **2016**, *511*, 65.
[63] T. Chen, W. Wu, H. Xiao, Y. Chen, M. Chen, J. S. Li, *ACS Macro Lett.* **2016**, *10*, 55.
[64] F. Jia, X. Liu, L. Li, S. Mallapragada, B. Narasimhan, Q. Wang, *J. Controlled Release* **2013**, *172*, 1020.
[65] A. Mageswari, R. Srinivasan, P. Subramanian, N. Ramesh, K. M. Gothandam, in *Sustainable Agriculture Reviews*, Vol. 23 (Eds: S. Ranjan, N. Dasgupta, E. Lichtfouse), Springer, Cham, Switzerland **2016**, pp. 31-71.
[66] C. Fornaguera, C. Solans, *J. Pers. Med.* **2017**, *7*, E2.
[67] X. Yang, F. Huang, X. Xu, Y. Liu, C. Ding, K. Wang, A. Guo, W. Li, J. Li, *Chem. Mater.* **2017**, *29*, 5663.
[68] M. J. Sailor, J. H. Park, *Adv. Mater.* **2012**, *24*, 3779.
[69] A. Kumari, R. Singla, A. Guliani, S. K. Yadav, *EXCLI J.* **2014**, *13*, 265.
[70] P. Heera, S. Shanmugam, *Int. J. Curr. Microbiol. Appl. Sci.* **2015**, *4*, 379.
[71] X.Yang, Z. Li, H. Xiao, N. Wang, Y. Li, X. Xu, Z. Chen, H. Tan, J. Li, *Adv. Funct. Mater.* **2018**, *28*, 1802730.
[72] N. Bertrand, J. Wu, X. Xu, N. Kamaly, O. C. Farokhzad, *Adv. Drug Delivery Rev.* **2014**, *66*, 2.
[73] Y. T. Kim, M. E. Lobatto, T. Kawahara, B. L. Chung, A. J. Mieszawska, B. L. Sanchez-Gaytan, F. Fay, M. L. Senders, C. Calcagno, J. Becraft, M. T. Saung, R. E. Gordon, E. S. G. Stroes, M. Ma, O. C. Farokhzad, Z. A. Fayad, W. J. M. Mulder, R. Langer, *Proc. Natl. Acad. Sci. U. S. A.* **2014**, *111*, 1078.
[74] E. J. Chung, *Exp. Biol. Med.* **2016**, *241*, 891.
[75] S. Wilhelm, A. J. Tavares, Q. Dai, S. Ohta, J. Audet, H. F. Dvorak, W. C. W. Chan, *Nat. Rev. Mater.* **2016**, *1*, 16014.
[76] R. Langer, N. Peppas, *J. Macromol. Sci., Polym. Rev.* **1983**, *23*, 61.
[77] R. A. Siegel, M. J. Rathbone, in *Advances in Delivery Science and Technology*, Vol. 4 (Eds : J. Siepmann, R. Siegel, M. Rathbone), Springer, Boston, US **2012**, pp. 19-43.
[78] S. Mura, J. Nicolas, P. Couvreur, *Nat. Mater.* **2013**, *12*, 991.
[79] J. H. Lee, Y. Yeo, *Chem. Eng. Sci.* **2015**, *125*, 75.

[80] S. Cao, Y. Liu, H. Shang, S. Li, J. Jiang, X. Zhu, P. Zhang, X. Wang, J. Li, *J. Controlled Release* **2017**, *256*, 182.
[81] W. Wu, J. Wang, Z. Lin, X. Li, J. S. Li, *Macromol. Rapid Commun*. **2014**, *35*, 1679.
[82] W. Wu, M. Chen, J. Wang, Q. Zhang, S. Li, Z. Li, J. S. Li, *RSC Adv.* **2014**, *4*, 30780.
[83] S. Li, W. Wu, K. Xiu, F. Xu, Z. Li, J. S. Li, *J. Biomed. Nanotechnol*. **2014**, *10*, 1480.
[84] W. Wu, L. Luo, Y. Wang, Q. Wu, H. B. Dai, J. S. Li, C. Durkan, N. Wang, G. X. Wang, *Theranostics* **2018**, *8*, 3038.
[85] J. C. Stendahl, A. J. Sinusas, *J. Nucl. Med.* **2015**, *56*, 1469.
[86] S. Sinharay, M. D. Pagel, *Annu. Rev. Anal. Chem.* **2016**, *9*, 95.
[87] P. Hauff, M. Reinhardt, S. Foster, in *Handb. Exp. Pharmacol.*, Vol. 185 (Eds: W. Semmler, M. Schwaiger), Springer, Berlin, UK **2008**, pp. 223-245.
[88] M. A. Calfon, A. Rosenthal, G. Mallas, A. Mauskapf, R. N. Nudelman, V. Ntziachristos, F. A. Jaffer, *J. Visualized Exp.* **2011**, *54*, 2257.
[89] J. Weber, P. C. Beard, S. E. Bohndiek, *Nat. Methods* **2016**, *13*, 639.
[90] J. Kim, N. Lee, T. Hyeon, *Philos. Trans. R. Soc., A* **2017**, *375*, 20170022.
[91] P. Pedrosa, R. Vinhas, A. Fernandes, P. V. Baptista, *Nanomaterials* **2015**, *5*, 1853.
[92] K. Li, H. Nejadnik, H. E. Daldrup-Link, *Drug Discovery Today* **2017**, *22*, 1421.
[93] M. Zhou, S. Song, J. Zhao, M. Tian, C. Li, *J. Mater. Chem. B* **2015**, *3*, 8939.
[94] W. N. Nowak, J. Deng, X. Z. Ruan, Q. Xu, *Arterioscler., Thromb., Vasc. Biol.* **2017**, *37*, e41.
[95] J. A. Leopold, J. Loscalzo, *Drug Discovery Today*: *Ther. Strategies* **2008**, *5*, 5.
[96] Y. Mikhed, A. Daiber, S. Steven, *Int. J. Mol. Sci.* **2015**, *16*, 15918.
[97] H. Li, U. Förstermann, *Curr. Opin. Pharmacol.* **2013**, *13*, 161.
[98] C. Kim, J. Y. Kim, J. H. Kim, *BMB Rep.* **2008**, *41*, 555.
[99] S. J. Nicholls, S. L. Hazen, *Arterioscler., Thromb., Vasc. Biol.* **2005**, *25*, 1102.
[100] M. G. Battelli, L. Polito, A. Bolognesi, *Atherosclerosis* **2014**, *237*, 562.
[101] A. Konior, A. Schramm, M. Czesnikiewicz-Guzik, T. J. Guzik, *Antioxid. Redox Signaling* **2014**, *20*, 2794.
[102] H. Li, S. Horke, U. Förstermann, *Trends Pharmacol. Sci.* **2013**, *34*, 313.
[103] H. Yang, L. J. Roberts, M. J. Shi, L. C. Zhou, B. R. Ballard, A. Richardson, Z. M. Guo*, Circ. Res.* **2004**, *95*, 1075.
[104] B. Chen, W. Wang, T. Shen, R. Qi, *PLoS One* **2013**, *8*, e76226.
[105] F. Cheng, M. Torzewski, A. Degreif, H. Rossmann, A. Canisius, K. J. Lackner, *PLoS One* **2013**, *8*, e72063.
[106] R. Sarangarajan, S. Meera, R. Rukkumani, P. Sankar, G. Anuradha, *Asian Pac. J. Trop. Med*. **2017**, *10*, 1111.
[107] W. Droge, *Physiol. Rev.* **2002**, *82*, 47.
[108] S. Lee, N. Murthy, *Biochem. Biophys. Res. Commun*. **2007**, *360*, 275.
[109] L. Bixenmann, J. He, M. Liang, W. Tremel, *Prog. Biochem. Biophys.* **2018**, *45*, 148.
[110] S. Rajeshkumar, P. Naik, *Biotechnology Reports* **2018**, *17*, 1.
[111] Y. Wang, L. Li, W. Zhao, Y. Dou, H. An, H. Tao, X. Xu, Y. Jia, S. Lu, J. Zhang, H. Hu, *ACS Nano* **2018**, *12*, 8943.
[112] S. W. Ryter, S. M. Cloonan, A. M. K. Choi, *Mol. Cells* **2013**, *36*, 7.
[113] M. O. J. Grootaert, L. Roth, D. M. Schrijvers, G. R. Y. De Meyer, W. Martinet, *Oxid. Med. Cell. Longevity* **2018**, *2018*, 1.
[114] W. Gao, Y. Zhao, X. Li, Y. Sun, M. Cai, W. Cao, Z. Liu, L. Tong, G. Cui, B. Tang, *Chem. Sci.* **2018**, *9*, 439.
[115] Y. C. Kim, K. L. Guan, *J. Clin. Invest.* **2015**, *125*, 25.
[116] X. Wang, L. Li, X. Niu, X. Dang, P. Li, L. Qu, X. Bi, Y. Gao, Y. Hu, M. Li, W. Qiao, Z. Peng, L. Pan, *DNA Cell Biol.* **2014**, *33*, 198.
[117] Y. Dou, Y. Chen, X. Zhang, X. Xu, Y. Chen, J. Guo, D. Zhang, R. Wang, X. Li, J. Zhang, *Biomaterials* **2017**, *143*, 93.

[118] A. Tawakol, A. P. Castano, F. Anatelli, G. Bashian, J. Stern, T. Zahra, F. Gad, S. Chirico, A. Ahmadi, A. J. Fischman, J. E. Muller, M. R. Hamblin, *J. Biomed. Opt.* **2006**, *11*, 021008.
[119] M. Jain, M. Zellweger, G. Wagnières, H. van den Bergh, S. Cook, M. N. Giraud, *Cardiovasc. Ther.* **2017**, *35*, e12238.
[120] H. Kim, Y. Kim, I. H. Kim, K. Kim, Y. Choi, *Theranostics* **2014**, *4*, 1.
[121] N. A. Jager, B. M. W. de Vries, J. L. Hillebrands, N. J. Harlaar, R. A. Tio, R. H. J. A. Slart, G. M. van Dam, H. H. Boersma, C. J. Zeebregts, J. Westra, *Mol. Imaging Biol.* **2016**, *18*, 283.
[122] R. Stern, M. J. Jedrzejas, *Chem. Rev.* **2006**, *106,* 818.
[123] D. Jiang, J. Liang, P. W. Noble, *Annu. Rev. Cell Dev. Biol.* **2007**, *23*, 435.
[124] C. F. Zhao, D. M. Herrington, *Am. J. Cardiovasc. Dis.* **2016**, *6*, 163.
[125] T. Quillard, H. A. Araújo, G. Franck, Y. Tesmenitsky, P. Libby, *Arterioscler., Thromb., Vasc. Biol.* **2014**, *34*, 1179.
[126] M. Aikawa, E. Rabkin, Y. Okada, S. J. Voglic, S. K. Clinton, C. E. Brinckerhoff, G. K. Sukhova, P. Libby, *Circulation* **1998**, *97*, 2433.
[127] V. Hugenberg, S. Wagner, K. Kopka, M. Schäfers, R. C. Schuit, A. D. Windhorst, S. Hermann, *J. Med. Chem.* **2017**, *60*, 307.
[128] T. Quillard, Y. Tesmenitsky, K. Croce, R. Travers, E. Shvartz, K. C. Koskinas, G. K. Sukhova, E. Aikawa, M. Aikawa, P. Libby, *Arterioscler., Thromb., Vasc. Biol.* **2011**, *31*, 2464.
[129] S. Fujimoto, D. Hartung, S. Ohshima, D. S. Edwards, J. Zhou, P. Yalamanchili, M. Azure, A. Fujimoto, S. Isobe, Y. Matsumoto, H. Boersma, N. Wong, J. Yamazaki, N. Narula, A. Petrov, J. Narula, *J. Am. Coll. Cardiol*. **2008**, *52*, 1847.
[130] S. Hermann, A. Starsichova, B. Waschkau, M. Kuhlmann, C. Wenning, O. Schober, M. Schäfers, *J. Nucl. Cardiol*. **2012**, *19*, 609.
[131] M. M. Sadeghi, D. K. Glover, G. M. Lanza, Z. A. Fayad, L. L. Johnson, *J. Nucl. Med.* **2010**, *51*, 51S.
[132] M. Schäfers, O. Schober, S. Hermann, *J. Nucl. Med.* **2010**, *51*, 663.
[133] A. C. Newby, *Curr. Opin. Lipidol.* **2006**, *17*, 556.
[134] E. Oviedo-Orta, A. Bermudez-Fajardo, S. Karanam, U. Benbow, A. C. Newby, *Immunology* **2008**, *124*, 42.
[135] G. K. Hansson, P. Libby, I. Tabas, *J. Intern. Med.* **2015**, *278*, 483.
[136] J. P. G. Sluijter, W. P. C. Pulskens, A. H. Schoneveld, E. Velema, C. F. Strijder, F. Moll, J. P. de Vries, J. Verheijen, R. Hanemaaijer, D. P. V. de Kleijn, G. Pasterkamp, *Stroke* **2006**, *37*, 235.
[137] M. J. Hobeika, R. W. Thompson, B. E. Muhs, P. C. Brooks, P. J. Gagne, *J. Vasc. Surg.* **2007**, *45*, 849.
[138] N. Hakimzadeh, V. A. Pinas, G. Molenaar, V. de Waard, E. Lutgens, B. L. F. van Eck-Smit, K. de Bruin, J. J. Piek, J. L. H. Eersels, J. Booij, H. J. Verberne, A. D. Windhorst, *PLoS One* **2017**, *12*, e0187767.
[139] H. Qin, Y. Zhao, J., Zhang, X. Pan, S. Yang, D. Xing, *Nanomedicine* **2016**, *12*, 1765.
[140] A. Müller, S. D. Krämer, R. Meletta, K. Beck, S. V. Selivanova, Z. Rancic, P. A. Kaufmann, B. Vos, J. Meding, T. Stellfeld, T. K. Heinrich, M. Bauser, J. Hütter, L. M. Dinkelborg, R. Schibli, S. M. Ametamey, *Nucl. Med. Biol.* **2014**, *41*, 562.
[141] L. Zhao, E. Lee, A. M. Zukas, M. K. Middleton, M. Kinder, P. S. Acharya, J. A. Hall, D. J. Rader, E. Puré, *Arterioscler., Thromb., Vasc. Biol.* **2008**, *28*, 1283.
[142] C. A. Cuff, D. Kothapalli, I. Azonobi, S. Chun, Y. Zhang, R. Belkin, C. Yeh, A. Secreto, R. K. Assoian, D. J. Rader, E. Puré, *J. Clin. Invest.* **2001**, *108*, 1031.
[143] D. Hägg, S. Sjöberg, L. M. Hultén, B. Fagerberg, O. Wiklund, A. Rosengren, L. M. S. Carlsson, J. Borén, P. A. Svensson, A. Krettek, *Atherosclerosis* **2007**, *190*, 291.
[144] F. D. Kolodgie, A. P. Burke, A. Farb, D. K. Weber, R. Kutys, T. N. Wight, R. Virmani, *Arterioscler., Thromb., Vasc. Biol.* **2002**, *22*, 1642.
[145] M. Jain, Q. He, W. S. Lee, S. Kashiki, L. C. Foster, J. C. Tsai, M. E. Lee, E. Haber, *J. Clin. Invest.* **1996**, *97*, 596.

[146] G. Y. Lee, J. H. Kim, G. T. Oh, B. H. Lee, I. C. Kwon, I. S. Kim, *J. Controlled Release* **2011**, *155*, 211.
[147] M. Zhang, J. He, C. Jiang, W. Zhang, Y. Yang, Z. Wang, J. Liu, *Int. J. Nanomed.* **2017**, *12*, 533.
[148] L. Liu, H. He, M. Zhang, S. Zhang, W. Zhang, J. Liu, *Biomaterials* **2014**, *35*, 8002.
[149] R. Kuai, D. Li, Y. E. Chen, J. J. Moon, A. Schwendeman, *ACS Nano* **2016**, *10*, 3015.
[150] W. Zhang, H. He, J. Liu, J. Wang, S. Zhang, S. Zhang, Z. Wu, *Biomaterials* **2013**, *34*, 306.
[151] A. Ji, J. M. Wroblewski, L. Cai, M. C. de Beer, N. R. Webb, D. R. van der Westhuyzen. *J. Lipid Res.* **2012**, *53*, 446.
[152] Y. Zhao, Z. He, H. Gao, H. Tang, J. He, Q. Guo, W. Zhang, J. Liu, *Biomacromolecules* **2018**, *19*, 2944.
[153] I. Abd-Elrahman, K. Meir, H. Kosuge, Y. Ben-Nun, T. W. Sadan, C. Rubinstein, Y. Samet, M. V. McConnell, G. Blum, *Stroke* **2016**, *47*, 1101.
[154] S. M. Shon, Y. Choi, J. Y. Kim, D. K. Lee, J. Y. Park, D. Schellingerhout, D. E. Kim, *Arterioscler., Thromb., Vasc. Biol.* **2013**, *33*, 1360.
[155] Z. Chen, K. W. Woodburn, C. Shi, D. C. Adelman, C. Rogers, D. I. Simon, *Arterioscler., Thromb., Vasc. Biol.* **2001**, *21*, 759.
[156] J. E. Muller, *J. Am. Coll. Cardiol.* **2008**, *52*, 1033.
[157] W. M. Sharman, C. M. Allen, J. E. van Lier, *Drug Discovery Today* **1999**, *4*, 507.
[158] D. E. Kim, J. Y. Kim, D. Schellingerhout, S. M. Shon, S. W. Jeong, E. J. Kim, W. K. Kim, *Mol. Imaging* **2009**, *8*, 291.
[159] D. S. Leake, *Atherosclerosis* **1997**, *129*, 149.
[160] L. M. Hultén, M. Levin, *Curr. Opin. Lipidol.* **2009**, *20*, 409.
[161] S. Parathath, Y. Yang, S. Mick, E. A. Fisher, *Trends Cardiovasc. Med.* **2013**, *23*, 80.
[162] K. Öörni, K. Rajamäki, S. D. Nguyen, K. Lähdesmäki, R. Plihtari, M. Lee-Rueckert, P. T. Kovanen, *J. Lipid Res.* **2015**, *56*, 203.
[163] M. Naghavi, R. John, S. Naguib, M. S. Siadaty, R. Grasu, K. C. Kurian, W. B. van Winkle, B. Soller, S. Litovsky, M. Madjid, J. T. Willerson, W. Casscells, *Atherosclerosis* **2002**, *164*, 27.
[164] S. Ohkuma, B. Poole, *Proc. Natl. Acad. Sci. U. S. A.* **1978**, *75*, 3327.
[165] C. Tang, D. Amin, P. B. Messersmith, J. E. Anthony, R. K. Prud'homme, *Langmuir* **2015**, *31*, 3612.
[166] S. Sungur, A. Uzar, *Spectrochim. Acta, Part A* **2008**, *69*, 225.
[167] X. Yang, P. Huang, H. Wang, S. Cai, Y. Liao, Z. Mo, X. Xu, C. Ding, C. Zhao, J. Li, *Colloids Surf., B* **2017**, *160*, 136.
[168] D. Park, Y. Cho, S. H. Goh, Y. Choi, *Chem. Commun.* **2014**, *50*, 15014.
[169] M. K. Gupta, S. H. Lee, S. W. Crowder, X. Wang, L. H. Hofmeister, C. E. Nelson, L. M. Bellan, C. L. Duvalla, H. J. Sung, *J. Mater. Chem. B* **2015**, *3*, 7271.
[170] J. J. Chiu, S. Chien, *Physiol. Rev.* **2011**, *91*, 327.
[171] Z. Teng, G. Canton, C. Yuan, M. Ferguson, C. Yang, X. Huang, J. Zheng, P. K. Woodard, D. Tang, *J. Biomech. Eng.* **2010**, *132*, 031007.
[172] N. Korin, M. Kanapathipillai, B. D. Matthews, M. Crescente, A. Brill, T. Mammoto, K. Ghosh, S. Jurek, S. A. Bencherif, D. Bhatta, A. U. Coskun, C. L. Feldman, D. D. Wagner, D. E. Ingber, *Science* **2012**, *337*, 738.
[173] Y. Chen, K. Zhang, J. Qiu, S. He, J. Huang, L. Huang, D. Jia, B. Ling, D. Sun, X. Xie, T. Yin, G. Wang, *Mol. Cell. Biomech.* **2017**, *14*, 83.
[174] S. P. Jackson, *Blood* **2007**, *109*, 5087.
[175] T. N. Durrant, M. T. van den Bosch, I. Hers, *Blood* **2017**, *130*, 1607.
[176] M. N. Holme, I. A. Fedotenko, D. Abegg, J. Althaus, L. Babel, F. Favarger, R. Reiter, R. Tanasescu, P. L. Zaffalon, A. Ziegler, B. Müller, T. Saxer, A. Zumbuehl, *Nat. Nanotechnol.* **2012**, *7*, 536.
[177] E. Hemmer, A. Benayas, F. Légaréa, F. Vetrone, *Nanoscale Horiz.* **2016**, *1*, 168.

[178] S. He, J. Song, J. Qu, Z. Cheng, *Chem. Soc. Rev.* **2018**, *47*, 4258.
[179] Z. Zhang, J. Wang, C. Chen, *Adv. Mater.* **2013**, *25,* 3869.
[180] V. Shanmugam, S. Selvakumar, C. S. Yeh, *Chem. Soc. Rev*. **2014**, *43*, 6254.
[181] A. N. Kharlamov, A. E. Tyurnina, V. S. Veselova, O. P. Kovtun, V. Y. Shur, J. L. Gabinsky, *Nanoscale* **2015**, *7*, 8003.
[182] W. Gao, Y. Sun, M. Cai, Y. Zhao, W. Cao, Z. Liu, G. Cui, B. Tang, *Nat. Commun.* **2018**, *9*, 231.
[183] X. B. Han, X. H. Li, Y. Q. Jiang, H. Wang, X. S. Li, J. Y. Kou, Y. H. Zheng, Z. N. Liu, H. Li, J. Li, D. Dou, Y. Wang, Y. Tian, L. M. Yang, *Cell Death Dis.* **2017**, *8*, e2864.
[184] T. Zako, H. Hyodo, K. Tsuji, K. Tokuzen, H. Kishimoto, M. Ito, K. Kaneko, M. Maeda, K. Soga, *J. Nanomater.* **2010**, *2010*, 1.
[185] B. G. Yi, O. K. Park, M. S. Jeong, S. H. Kwon, J. I. Jung, S. Lee, S. Ryoo, S. E. Kim, J. W. Kim, W. J. Moon, K. Park, *Int. J. Biol. Macromol.* **2017**, *97*, 181.
[186] Food and Drug Administration (FDA) : Indocyanine Green (IC-GREEN™). https://www.accessdata.fda.gov/drugsatfda_docs/label/2006/011525s017lbl.pdf. Accessed on 16 August 2018.
[187] W. R. Chen, H. Liu, J. W. Ritchey, K. E. Bartels, M. D. Lucroy, R. E. Nordquist, *Cancer Res.* **2002**, *62*, 4295.
[188] C. Shirata, J. Kaneko, Y. Inagaki, T. Kokudo, M. Sato, S. Kiritani, N. Akamatsu, J. Arita, Y. Sakamoto, K. Hasegawa, N. Kokudo, *Sci. Rep.* **2017**, *7*, 13958.
[189] C. Abels, S. Fickweiler, P. Weiderer, W. Bäumler, F. Hofstädter, M. Landthaler, R. M. Szeimies, *Arch. Dermatol. Res.* **2000**, *292*, 404.
[190] S. Ma, S. M. Motevalli, J. Chen, M. Q. Xu, Y. Wang, J. Feng, Y. Qiu, D. Han, M. Fan, M. Ding, L. Fan, W. Guo, X. J. Liang, F. Cao, *Theranostics* **2018**, *8*, 3693.
[191] T. Lajunen, L. S. Kontturi, L. Viitala, M. Manna, O. Cramariuc, T. Róg, A. Bunker, T. Laaksonen, T. Viitala, L. Murtomäki, A. Urtti, *Mol. Pharmaceutics* **2016**, *13*, 2095.
[192] A. K. Kirchherr, A. Briel, K. Mäder, *Mol. Pharmaceutics* **2009**, *6*, 480.
[193] J. C. Kraft, R. J. Ho, *Biochemistry* **2014**, *53*, 1275.
[194] V. Paefgen, D. Doleschel, F. Kiessling, *Front. Pharmacol.* **2015,** *6*, 197.
[195] R. Gramiak, P. M. Shah, *Invest. Radiol.* **1968**, *3*, 356.
[196] I. Lentacker, I. D. Cock, R. Deckers, S. C. D. Smedt, C. T. W. Moonen, *Adv. Drug Delivery Rev.* **2014**, *72*, 49.
[197] B. H. Lammertink, C. Bos, R. Deckers, G. Storm, C. T. W. Moonen, J. M. Escoffre, *Front. Pharmacol.* **2015**, *6*, 138.
[198] A. W. Appis, M. J. Tracy, S. B. Feinstein, *Echo. Res. Pract.* **2015**, *2*, R55.
[199] H. Shankaran, P. Alexandridis, S. Neelamegham, *Blood* **2003**, *101*, 2637.
[200] T. Yago, J. Lou, T. Wu, J. Yang, J. J. Miner, L. Coburn, J. A. López, M. A. Cruz, J. F. Dong, L. V. McIntire, R. P. McEver, C. Zhu, *J. Clin. Invest.* **2008**, *118*, 3195.
[201] O. J. T. McCarty, R. B. Conley, W. Shentu, G. W. Tormoen, D. Zha, A. Xie, Y. Qi, Y. Zhao, C. Carr, T. Belcik, D. R. Keene, P. G. de Groot, J. R. Lindner, *JACC Cardiovasc. Imaging* **2010**, *3*, 947.
[202] F. Yan, Y. Sun, Y. Mao, M. Wu, Z. Deng, S. Li, X. Liu, L. Xue, H. Zheng, *Theranostics* **2018**, *8*, 1879.
[203] X. Zhang, K. Zhao, J. Wang, S. Bai, S. Jiao, J. Zhang, L. Yu, *New J. Chem.* **2016**, *40*, 1256.
[204] F. Moccetti, C. C. Weinkauf, B. P. Davidson, J. T. Belcik, E. R. Marinelli, E. Unger, J. R. Lindner, *Ultrasound Med. Biol.* **2018**, *44*, 1155.
[205] L. Petrov, M. U. Kaikkonen, T. Heikura, T. Wirth, E. Aavik, K. Airenne, S. Yla-Herttuala, *Mol. Ther.* **2008**, *16*, S55.
[206] K. Wang, B. Guo, F. Zhang, X. Wang, J. Yang, Y. Zheng, C. Wu, *J. Nanosci*. *Nanotechnol*. **2016**, *16*, 7611.
[207] A. Ranga, Y. Agarwal, K. J. Garg, *Indian J. Radiol. Imaging* **2017**, *27*, 141.
[208] M. Rogosnitzky, S. Branch, *Biometals* **2016**, *29*, 365.

[209] I. A. Mendichovszky, S. D. Marks, C. M. Simcock, O. E. Olsen, *Pediatr. Radiol*. **2008**, *38*, 489.
[210] Y. X. Wang, S. Xuan, M. Port, J. M. Idee, *Curr. Pharm. Des.* **2013**, *19*, 6575.
[211] M. Bietenbeck, A. Florian, C. Faber, U. Sechtem, A. Yilmaz, *Int. J. Nanomedicine* **2016**, *11*, 3191.
[212] A. L. Cortajarena, D. Ortega, S. M. Ocampo, A. Gonzalez-García, P. Couleaud, R. Miranda, C. Belda-Iniesta, A. Ayuso-Sacido, *Nanobiomedicine* **2014**, *1*, 2.
[213] S. H. Nasr, A. Tonson, M. H. El-Dakdouki, D. C. Zhu, D. Agnew, R. Wiseman, C. Qian, X. Huang, *ACS Appl. Mater. Interfaces* **2018**, *10*, 11495.
[214] T. Sha, C. Qi, W. Fu, J. Hao, L. Gong, H. Wu, Q. Zhang, *Exp. Ther. Med.* **2016**, *12*, 141.
[215] C. Qi, L. Deng, D. Li, W. Wu, L. Gong, Y. Li, Q. Zhang, T. Zhang, C. Zhang, Y. Zhang, *PLoS One* **2015**, *10*, e0125677.
[216] K. Stach, X. D. Nguyen, S. Lang, E. Elmas, C. Weiss, M. Borggrefe, J. Fischer, T. Kälsch, *Cardiol. J.* **2012**, *19*, 20.
[217] Z. Xu, S. Zhao, H. Zhou, H. Ye, J. Li, *Clin. Chem.* **2004**, *50*, 750.
[218] Y. Dong, H. Chen, C. Chen, X. Zhang, X. Tian, Y. Zhang, Z. Shi, Q. Liu, *J. Biomed. Nanotechnol.* **2016**, *12*, 1245.
[219] S. Chandramouli, S. Sanjana, S. Swathi, in *Proc. IFMBE 5th* (Eds: V. V. Toi, T. H. L. Phuong), Vietnam National Universities HCM City (VNU-HCM) and International University of VNU-HCM, Vietnam **2015**.
[220] J. B. Weaver, X. Zhang, E. Kuehlert, S. Toraya-Brown, D. B. Reeves, I. M. Perreard, S. Fiering, *Nanotechnology* **2013**, *24*, 325502.
[221] D. B. Reeves, J. B. Weaver, *J. Appl. Phys.* **2012**, *112*, 124311.
[222] K. Hayashi, K. Ono, H. Suzuki, M. Sawada, M. Moriya, W. Sakamoto, T. Yogo, *ACS Appl. Mater. Interfaces* **2010**, *2*, 1903.
[223] R. Cheng, F. H. Meng, C. Deng, H. A. Klok, Z. Y. Zhong, *Biomaterials* **2013**, *34*, 3647.
[224] M. Karimi, A. Ghasemi, P. S. Zangabad, R. Rahighi, S. M. M. Basri, H. Mirshekari, M. Amiri, Z. S. Pishabad, A. Aslani, M. Bozorgomid, D. Ghosh, A. Beyzavi, A. Vaseghi, A. R. Aref, L. Haghani, S. Bahramia, M. R. Hamblin, *Chem. Soc. Rev.* **2016**, *45*, 1457.
[225] Y. Wang, Y. Zhong, L. Luo, X. Li, T. Yin, J. Huang, X. Zhang, W. Wu, G. Wang, *Mater. Chem. Phys.* **2018**, *211*, 177.
[226] R. B. Altman, Q. Zheng, Z. Zhou, D. S. Terry, J. D. Warren, S. C. Blanchard, *Nat. Methods* **2012**, *9*, 428.
[227] X. Zhang, S. Bloch, W. Akers, S. Achilefu, *Curr. Protoc. Cytom.* **2012**, *60*, 12271.
[228] S. L. Gibbs, *Quant. Imaging Med. Surg.* **2012**, *2*, 177.
[229] P. P. Ghoroghchian, M. J. Therien, D. A. Hammer, *Wiley Interdiscip. Rev.: Nanomed. Nanobiotechnol.* **2009**, *1*, 156.
[230] C. L. Tarver, M. Pusey, *Acta Crystallogr., Sect. F: Struct. Biol. Commun.* **2017**, *73*, 657.
[231] N. Kosaka, M. Ogawa, P. L. Choyke, H. Kobayashi, *Future Oncol.* **2009**, *5*, 1501.
[232] J. A. Ronald, J. W. Chen, Y. Chen, A. M. Hamilton, E. Rodriguez, F. Reynolds, R. A. Hegele, K. A. Rogers, M. Querol, A. Bogdanov, R. Weissleder, B. K. Rutt, *Circulation* **2009**, *120*, 592.
[233] H. Wei, O. T. Bruns, M. G. Kaul, E. C. Hansen, M. Barch, A. Wiśniowska, O. Chen, Y. Chen, N. Li, S. Okada, J. M. Cordero, M. Heine, C. T. Farrar, D. M. Montana, G. Adam, H. Ittrich, A. Jasanoff, P. Nielsen, M. G. Bawendi, *Proc. Natl. Acad. Sci. U. S. A.* **2017**, *114*, 2325.
[234] T. Vangijzegem, D. Stanicki, S. Boutry, Q. Paternoster, L. V. Elst, R. N. Muller, S. Laurent, *Nanotechnology* **2018**, *29*, 265103.
[235] Y. Bao, J. A. Sherwood, Z. Sun, *J. Mater. Chem. C* **2018**, *6*, 1280.
[236] N. V. S. Vallabani, S. Singh, *3 Biotech* **2018**, *8*, 279.
[237] E. B. Peters, N. D. Tsihlis, M. R. Karver, S. M. Chin, B. Musetti, B. T. Ledford, E. M. Bahnson, S. I. Stupp, M. R. Kibbe, *Adv. Healthcare Mater.* **2019**, *8*, e1801545.
[238] S. H. Hong, Y. Li, J. B. Eom, Y. Choi, *Quant. Imaging Med. Surg.* **2018**, *8*, 733.

[239] H. Hu, H. Zhou, J. Du, Z. Q. Wang, L. An, H. Yang, F. H. Li, H. X. Wu, S. P. Yang, *J. Mater. Chem.* **2011**, *21*, 6576.
[240] L. An, H. Hu, J. Du, J. Wei, L. Wang, H. Yang, D. Wu, H. Shi, F. Li, S. Yang, *Biomaterials* **2014**, *35*, 5381.
[241] P. L. Lin, R. J. Eckersley, E. A. H. Hall, *Adv. Mater.* **2009**, *21*, 3949.
[242] R. Ji, X. Li, C. Zhou, Q. Tian, C. Li, S. Xia, R. Wang, Y. Feng, W. Zhan, *Nanoscale* **2018**, *10*, 20246.
[243] J. W. Verjans, E. A. Osborn, G. J. Ughi, M. A. C. Press, E. Hamidi, A. P. Antoniadis, M. I. Papafaklis, M. F. Conrad, P. Libby, P. H. Stone, R. P. Cambria, G. J. Tearney, F. A. Jaffer, *JACC Cardiovasc. Imaging* **2016**, *9*, 1087.
[244] W. Xiong, P. Wang, J. Hu, Y. Jia, L. Wu, X. Chen, Q. Liu, X. Wang, *Sci. Rep.* **2015**, *5*, 17485.
[245] G. Y. Wan, Y. Liu, B. W. Chen, Y. Y. Liu, Y. S. Wang, N. Zhang, *Cancer Biol. Med.* **2016**, *13*, 325.
[246] H. Wang, P. Wang, L. Li, K. Zhang, X. Wang, Q. Liu, *Int. J. Biol. Sci.* **2015**, *11*, 1401.
[247] M. C. García, J. C. Cuggino, in *Stimuli Responsive Polymeric Nanocarriers for Drug Delivery Applications*, Vol. 1 (Eds: A. S. H. Makhlouf, N. Y. Abu-Thabit), Elsevier, Duxford, UK **2018**, pp. 321-341.
[248] Y. Liu, X. Chen, S. Li, Q. Guo, J. Xie, L. Yu, X. Xu, C. Ding, J. Li, J. Ding, *ACS Appl. Mater. Interfaces* **2017**, *9*, 23428.
[249] H. Shang, X. Chen, Y. Liu, L. Yu, J. Li, J. Ding, *Int. J. Pharm.* **2017**, *527*, 52.
[250] J. Xie, A. Li, J. Li, *Macromol. Rapid Commun.* **2017**, *38*, 1700413.
[251] E. S. Haswell, R. Phillips, D. C. Rees, *Structure* **2011**, *19*, 1356.
[252] C. C. Cruickshank, R. F. Minchin, A. C. L. Dain, B. Martinac, *Biophys. J.* **1997**, *73*, 1925.
[253] I. Iscla, C. Eaton, J. Parker, R. Wray, Z. Kovács, P. Blount, *Biosensors* **2013**, *3*, 171.
[254] B. J. Hong, A. Iscen, A. J. Chipre, M. M. Li, O. S. Lee, J. N. Leonard, G. C. Schatz, S. B. T. Nguyen, *J. Phys. Chem. Lett.* **2018**, *9*, 1133.
[255] L. M. Yang, H. Zheng, J. S. Ratnakar, B. Y. Adebesin, Q. N. Do, Z. Kovacs, P. Blount, *Small* **2018**, *14*, 1704256.
[256] Y. Nakayama, M. Mustapić, H. Ebrahimian, P. Wagner, J. H. Kim, M. S. A. Hossain, J. Horvat, B. Martinac, *Eur. Biophys. J.* **2015**, *44*, 647.
[257] A. D. Martinac, N. Bavi, O. Bavi, B. Martinac, *PloS One* **2017**, *12*, e0183822.